scientific reports

Check for updates

OPEN

Evaluation of heat transfer performance of a heat exchanger tube mounted with an I-rib twisted tape and twisted winglets

Wenxuan Qiu[1], Prachya Samruaisin[1], Varesa Chuwattanakul[2]✉, Naoki Maruyama[3,4], Masafumi Hirota[5] & Smith Eiamsa-ard[1]

This study aims to improve the efficiency of heat exchangers and explore the enhancement mechanism of the thermal performance characteristics of heat exchange tubes by I-rib twisted tapes and twisted winglets (I-RTTW) through experimental research and numerical simulation. The I-RTTW structure consists of a central I-type rib and an edge twisted winglet. The key geometric parameters of the edge twisted winglet include the wing depth ratio (*d/W* = 0.096, 0.13, 0.16), the wing width ratio (*w/W* = 0.096, 0.13, 0.16), and a fixed twist angle of 45°. The study uses air as the working fluid to systematically analyze the heat transfer performance of the I-RTTW over a range of Reynolds numbers (*Re*) of 6,000–20,000. The experimental results reveal that the I-RTTW significantly improves heat transfer through a dual mechanism. First, the edge twisted winglet effectively disrupts the fluid boundary layer by inducing secondary flows. Second, the central I-type rib can promote radial mixing of the fluid. Further in-depth analysis of the experimental data revealed that a greater winglet depth ratio (d/W) increases the longitudinal size of the cutting winglet, thereby disturbing the fluid more deeply and increasing boundary layer disruption. An increased winglet width ratio (*w/W*) significantly enhances the fluid mixing effect by expanding the lateral coverage, thereby reducing thermal resistance and enhancing heat transfer between the pipe wall and the fluid. In terms of flow resistance characteristics, a greater winglet depth ratio directly leads to an increased longitudinal size of the cutting winglet. This strengthens the disturbance of fluid, resulting in increased boundary layer separation and greater eddy losses. Similarly, an increased winglet width ratio leads to greater lateral flow resistance, so that the fluid needs to overcome a larger shear force and higher collision losses. This leads to an increased friction coefficient (*f*). In the current study, the heat transfer rate of a pipe equipped with I-RTTWs is about 7 to 26% and 68 to 99% higher than that of a pipe equipped with typical tape (TT) and the plain tube, respectively. The friction coefficient is 1.15–1.37 times and 3.46–4.12 times that of a TT and plain tube, respectively. The comprehensive thermal performance index of the pipe with an I-RTTW is as high as 1.29.

Keywords Heat exchanger, Heat transfer performance, I-rib twisted tape, Twisted winglet

List of symbols

A	Heat transfer area inside tube surface m^2
C_p	Specific heat, J/kg K
D	Diameter of test section, m
f	Friction factor, dimensionless
h	Convection heat transfer coefficient, W/ m^2 K
k	Conduction heat transfer coefficient, W/ m K
$\dot{m}$	Mass flow rate, kg/s

[1]School of Engineering and Industrial Technology, Mahanakorn University of Technology, Bangkok 10530, Thailand. [2]School of Engineering, King Mongkut's Institute of Technology Ladkrabang, Bangkok 10520, Thailand. [3]Engineering Innovation Unit, Graduate School of Regional Innovation Studies, Mie University, Tsu 514-8507, Mie, Japan. [4]Department of Mechanical Engineering, Faculty of Engineering, Mie University, Tsu 514-8507, Mie, Japan. [5]Department of Mechanical Engineering, Faculty of Engineering, Aichi Institute of Technology, Toyota 470-0392, Aichi, Japan. ✉email: varesa.ch@kmitl.ac.th

Nu	Nusselt number, dimensionless
P	Pressure, Pa
Pr	Prandtl number, dimensionless
Q	Heat transfer, W
Re	Reynolds number, ($\rho UD/\mu$) dimensionless
T	Temperature, K
$\widetilde{T}$	Average fluid temperature, K
W	Tape width, m
y	Twist length, m
U	Air velocity, m/s

Greek letters

α	Twist winglet angle, °
μ	Dynamic viscosity, kg/m^3
ρ	Density, kg/ m^3

Subscripts

b	Bulk
$conv$	Convection
i	Inlet
o	Outlet
w	Wall

Abbreviations

I-RTTW	I-rib twisted tape and twisted winglets
TPI	Thermal performance index
TT	Typical/Conventional twisted tape

Tube heat exchangers play a key role in energy-intensive industries such as power generation, chemical processing, and HVAC systems[1,2]. The International Energy Agency (IEA) predicts that global energy demand will increase 50% by 2050[3], which has led to a renewed focus on passive heat transfer enhancement technologies as cost-effective solutions for optimizing thermal systems. They can enhance thermal performance while effectively controlling pumping power losses. Among numerous passive enhancement strategies, swirl generators, particularly twisted tape inserts, have demonstrated unique advantages in enhancing heat transfer performance through flow pattern regulation[4]. These helical structures enhance heat transfer through two mechanisms: (1) generating longitudinal vortices that disrupt the development of boundary layers[5,6], and (2) increasing the tortuosity of fluid mixing paths[7]. Both mechanisms play a vital role in heat transfer enhancement.

Researchers have optimized the spiral structure parameters and geometric shape, strengthened the boundary layer disturbance, and promoted fluid mixing, significantly improving heat transfer performance. Different working fluids (water, nanofluids, air) were combined to enable enhanced heat transfer under various scenarios. Thejaraju et al.[1] designed airfoils of assorted sizes to induce multi-scale vortices that enhance fluid mixing. They showed excellent comprehensive performance in the high Reynolds number region. Experiments show that when Re = 30,000, a new airfoil strip (Para-Winglet Tape) has a 407% increased Nu compared to a plain tube, an 846% increased friction coefficient, and a comprehensive performance coefficient (POI) of 2.69. Altun et al.[2] introduced a sinusoidal waveform structure. At Re = 5,000, the twisted wavy tape with an amplitude of D/8 and a wave number of 3 had a 37% increased Nu and a 48% greater friction coefficient compared with a typical tape. It also had a comprehensive performance factor of 1.43. The design of this waveform significantly improves the heat transfer efficiency at low Reynolds numbers by enhancing fluid disturbance and secondary flow. Rubbi et al.[4] experimentally induced additional vortices through surface structures, significantly enhancing boundary layer disturbances and achieving performance optimization while maintaining high heat transfer. Numerical simulations showed that a twisted tape with a hemispherical extrusion surface (HES) increased the Nusselt number (Nu) by 69.4%. The friction coefficient increased by 149–188% compared with a plain tube at Re = 4,000–10,000, and the comprehensive performance coefficient reached 1.23. Samutpraphut et al.[5] found that a serrated structure formed local vortices through periodic flow resistance, further enhancing boundary layer disruption. The experimental results showed that when Re = 6,000, the Nu of the sawtooth twisted tape with a serration angle of 70° was 186.2% higher than that of a plain tube. The friction coefficient reached 0.135, and the comprehensive performance coefficient rose to 1.33. Abdulhamed et al.[6] experimentally demonstrated that fluid penetrates large pores to form additional mixed flows, significantly reducing resistance while enhancing heat transfer, breaking through the performance bottleneck of traditional twisted ribbons. The experiment found that twisted tapes with large pores (porosities of 1.3 and 2.7%) performed well under turbulent conditions (Re = 4,800–9,500). The Nusselt number increased by 87–97% compared to a plain tube, the friction coefficient was reduced by 70–94%, and the comprehensive performance coefficient reached 89%. Sedaghat et al.[8] found that adding a perforated structure to the traditional twisted tape not only maintained the vortex intensity but also effectively reduced pressure losses. The experimental results show that the Nusselt number of a 6-blade perforated twisted tape in the range of Re = 200–1,000 is 15.24% higher than that of a typical tape. The friction coefficient is reduced by 22.26%, and the comprehensive performance coefficient is increased by 18.07%. This design forms an additional mixed flow by penetrating the perforations, balancing heat transfer and flow resistance. Chuwattanakul et al.[9] found through experimental comparison that the fin structure superimposed a longitudinal vortex that significantly improved fluid mixing. At Re = 6,000, the Nusselt number of the forward-arranged 45° V-shaped rib broken V-ribbed twisted tape was 227% higher than that of a plain tube. Its friction coefficient was 4.4, and the comprehensive performance coefficient reached 1.38. Fetug et al.[10] experimentally demonstrated that superposition of a periodic alternating axis structure and baffle-induced longitudinal vortex significantly

improved the boundary layer distribution. Experimental results show that the combination of semi-alternating twisted tapes and cylindrical baffles performs well under laminar conditions (Re = 500–2,000). When the pitch ratio decreases from 5.77 to 1.77, the Nusselt number increases by 35–107% compared with a plain tube. The friction coefficient increases from 0.26 to 3.5 Pa, and the comprehensive performance coefficient is improved by 1.35–1.67 times. Heeraman et al.[11] induced additional vortices through a dimple structure, significantly enhancing the boundary layer disturbance, and achieved performance optimization while maintaining high heat transfer. Experiments have shown that when a twisted tape with a dimple diameter of 4.0 mm and D/H = 3.0 is used in a double-tube heat exchanger at Re = 13,987, the Nusselt number is increased by 111% compared with a bare tube. Its friction coefficient is 0.1033, and the comprehensive performance coefficient reaches 1.08. Thapa et al.[12] significantly enhanced the fluid mixing efficiency and optimized heat transfer improvement and flow resistance by inducing secondary flow boundary layer disturbance through perforations and an airfoil. Through MATLAB simulation, it was found that the composite structure with a twist ratio of 3.0, perforation ratio of 0.05, and airfoil ratio of 0.1, had a thermal efficiency of 84.27% at Re = 6,000. This was 29.27% higher than that of a plain tube. Thote et al.[13] significantly enhanced fluid mixing by inducing a working fluid to pass through a trapezoidal cutout to generate additional vortices and disturb boundary layers. This broke through the performance limitations of typical tape in low Reynolds number scenarios. Experiments have shown that the trapezoidal cutout twisted tape performs well under laminar conditions (Re = 830–1,990). When the twist ratio is 3.0, the Nusselt number is increased by 112–356% compared with a plain tube, the friction coefficient is 0.3126–0.4126, and the comprehensive performance coefficient reaches 1.55–3.56. Smaisim et al.[14] compared the performance differences between rotating and fixed twisted tapes. They found that the clockwise rotation increased Nusselt number by 20.2% compared with the fixed tape at Re = 1,000. A counterclockwise rotation further reduced the local thermal resistance by enhancing a reverse vortex. Eiamsa-ard et al.[15] significantly improved the boundary layer distribution by designing a multiple twisted tape structure to induce vortices. Their experiments showed that the Nusselt number of a 6-blade co-directional/counter-directional twisted tape bundle increased by 70.6% and the friction coefficient rose by 172.7% compared with a typical tape at Re = 6,000. Its comprehensive performance coefficient reached 1.33. The reverse arrangement further improved Nusselt number by 1.4–4.1% compared with the co-directional arrangement by enhancing fluid mixing and turbulence intensity, while the friction coefficient increased by only 3.0–7.6%. Promvonge et al.[16] reduced the pressure drop while maintaining high heat transfer by combining the turbulence of the airfoil and vortices generated by a twisted tape. The study found that by combining a 30° V-wing with a twin counter-twisted tape, the Nusselt number increased by 1.56–2.3 times compared to a bare tube in the range of Re = 5,300–24,000. The friction coefficient increased by 2.63–5.76 times, and the best comprehensive performance coefficient reached 1.76. Luo et al.[17] proposed an asymmetric two-co-twisting oval twisted tube structure. This design enhances the secondary flow intensity by periodically changing the flow channel cross-section. It exhibits excellent comprehensive performance in the laminar flow region. When the inner and outer tube twist ratio is 1.5, the Nusselt number is increased by 97% compared with a straight tube. The friction coefficient only increases by 43.7%, and the comprehensive performance coefficient reaches 1.75. Eiamsa-ard et al.[18] found that a twin delta-winged twisted-tape significantly improved the heat transfer of a heat exchanger tube. Compared with a traditional twisted tape, the traditional twisted tape-up achieves a better overall performance while maintaining high heat transfer by inducing stronger fluid collisions and longitudinal vortices. A smaller wingtip angle produces a more significant heat transfer enhancement. Eiamsa-ard et al.[19] designed a periodic alternating axis structure, which induces additional vortices and significantly improves the boundary layer distribution. The performance of twisted tape with uniform alternate length with a shorter alternating length is more significantly improved than that of conventional twisted tapes. Samruaisin et al.[20] experimentally designed a twisted tube surface that induced secondary flow and enhanced twisted band vortices, achieving compact structure optimization while maintaining high heat transfer. When the trapezoidal twisted tube and twisted band are combined at Re = 4,500–16,000, the Nusselt number is increased by 126–172% compared with a plain tube. The friction coefficient is increased by 8–12 times, and the comprehensive performance coefficient reaches 1.28. Chang et al.[21] experimentally achieved a balance between efficient heat transfer and pressure drop in a square tube by promoting fluid mixing through longitudinal vortices induced by ribs and grooves. Through numerical simulation and experiments, it was found that when Re = 10,000–50,000, the Nusselt number of the twisted belt with inclined ribs and grooves was improved by 3.8–4.2 times compared with a smooth tube. The friction coefficient increased by 32.5–40.2 times, and the comprehensive performance coefficient reached 1.31. Yu et al.[22] experimentally showed that a central hollow twisted tape performed best in a twisted elliptical tube. This design significantly reduced the flow resistance while maintaining high heat transfer by reducing the fluid blockage area. Its performance was improved by 10.06% compared with a traditional twisted tape. Abidi et al.[23] found that a combination of CuO nanofluid and perforated twisted tape increased the Nusselt number by 70% compared with pure water at Re = 10,000, and the pressure drop was only 3.5 Pa. Concurrently, the perforated structure significantly improved the performance coefficient by 1.6 through reduction of the flow blockage area. Ghasemian et al.[24] found that twisted tapes disrupt the boundary layer by enhancing swirl flow, achieving compact structural optimization while maintaining high heat recovery efficiency. Chen et al.[25] designed a method to form an additional mixed flow by penetrating a porous structure, which showed an excellent synergistic strengthening effect in the laminar flow region. Through two-phase flow simulation, it was found that when Re = 6,000, the Nu of the porous triple twisted tape was improved by 15–24% compared with the plain tube. The friction coefficient increased by only 12–22%, and the comprehensive performance coefficient reached 1.38. Chompookham et al.[26] designed a sawtooth structure to induce local eddy currents, balancing the heat transfer and pressure drop trade off in low Reynolds number scenarios. Experiments show that when Re = 5,114, the Nu of the sawtooth coil is 1.75 times higher than that of a plain tube. The friction coefficient is increased by 3.31 times. Hong et al.[27] designed a corrugated structure to induce the lateral vortex and superimpose swirls generated by the wire coil, which

significantly enhanced fluid mixing efficiency. Chithra et al.[28] found through numerical simulation that when a variable pitch twisted tape is used in a twisted square tube, at a Reynolds number of Re = 1,000, the Nusselt number is improved by 82% compared with a smooth tube. The friction coefficient is 3.01 times higher, and the comprehensive performance factor reaches 1.32. This design induces additional vortices through a periodic alternating axis structure, significantly improving the boundary layer distribution and performance by 15.7% compared with a traditional fixed pitch twisted tape. Nuntadusit et al.[29]studied the heat transfer and flow characteristics in several types of transverse perforated rib channels. Through experiments and numerical simulations, it was found that inclined perforated ribs significantly improved heat transfer downstream of the ribs. Compared with straight perforated ribs and solid ribs, their overall heat transfer performance was better. Larger inclination angles produced greater heat transfer enhancement. Eiamsa-ard et al.[30] studied the effects of inserting tandem wire coil elements in a square pipe on the heat transfer and friction characteristics under turbulent flow. The results showed that the coil can improve corner flow by inducing swirl to improve heat transfer. The thermal enhancement factor can reach 1.33 at low Reynolds numbers. Samruaisin et al.[20]studied the effect of combining a twisted tube and twisted tape on heat transfer, pressure drop, and thermal performance was studied, using a trapezoidal twisted tube and twisted tapes with different twist ratios. Pazarlıoğlu et al.[31] numerically analyzed expansion tubes with varying expansion angles combined with capsule-shaped dimple fins. Their results indicated a substantial increase in the average Nusselt number, accompanied by reduced entropy and enhanced exergy output. In a separate study, Pazarlıoğlu et al.[32] numerically investigated the anti-icing performance of a NACA0015 airfoil by varying jet-to-surface distance, jet angle, and slot jet aspect ratio. Simulations were carried out in ANSYS Fluent using the SST k–ω turbulence model with low-Re corrections. Results showed that an aspect ratio of 4.0 at H/d = 4.0 and α = 90° increased the average Nusselt number by 85.5% compared to a circular jet, albeit with a 307.9% rise in pressure drop. Despite this, the performance evaluation criterion remained constant at 1.14. The Nusselt number, friction factor, and thermal performance factor of the combined device are higher than those of a single twisted tube and a plain tube. As the twist ratio decreases, the heat transfer, friction loss, and thermal performance are enhanced.

Based on the effectiveness verification of twisted tapes as core elements for heat transfer enhancement in previous studies, this study innovatively constructed a composite structure of an I-rib twisted tape and twisted winglets. Experimental and numerical simulations explored the synergistic heat transfer enhancement mechanism. The composite structure achieves heat transfer enhancement through a dual action, as shown in Fig. 1: Swirling vortices and turbulence induced by the winglets on the pipe wall effectively disrupt boundary layer development and guide the fluid to the central area. Additionally, the I-ribs located in the middle of the pipe promote momentum exchange between the wall fluid and the core flow area by generating secondary swirling flows, forming a more uniform mixed flow field. The research variables include varying winglet depth ratios (d/W = 0.096, 0.13, and 0.16), wing width ratios (w/W = 0.096, 0.13, and 0.16), and a fixed twisted angle (45°). Normal air pressure was selected as the experimental working fluid. Systematic tests were conducted in the range of Re = 6,000–20,000, keeping other operating parameters consistent.

Experimental design

Continuous I-ribs with twisted tape winglets

A new heat transfer enhancement element used in this experimental, the I-rib twisted tape and twisted winglet (I-RTTW) composite structure is shown in Fig. 2. This structure achieves multi-scale control of the flow field in the tube to enhance the heat transfer performance through the coordinated design of edge cutting winglets, central I-ribs, and twisted spiral structures.

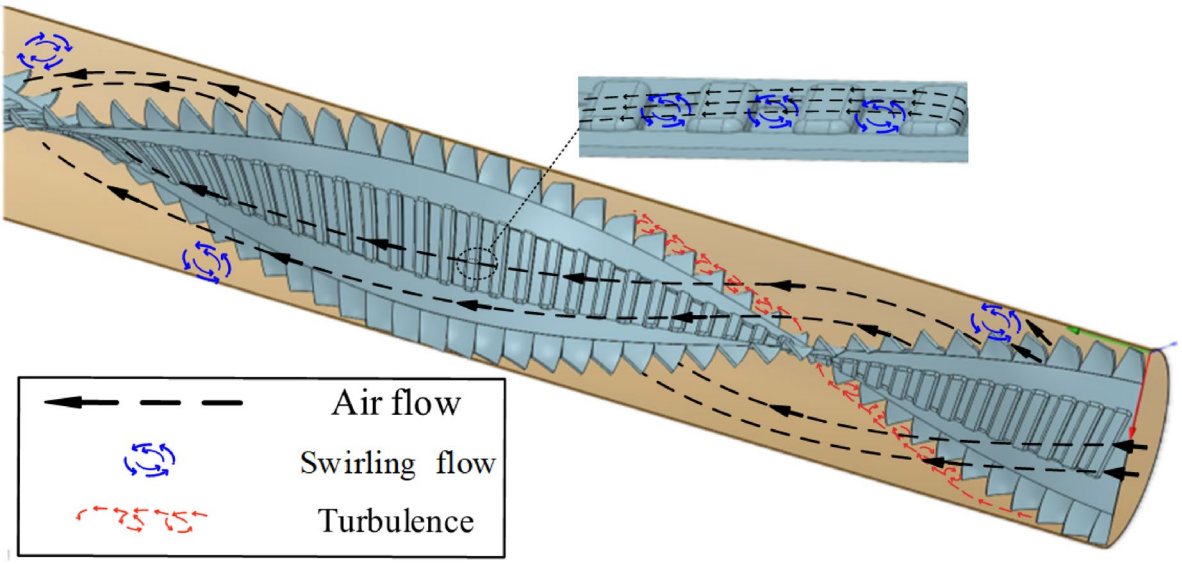

Fig. 1. Tube fitted with I-rib twisted tape and twisted winglets (I-RTTW).

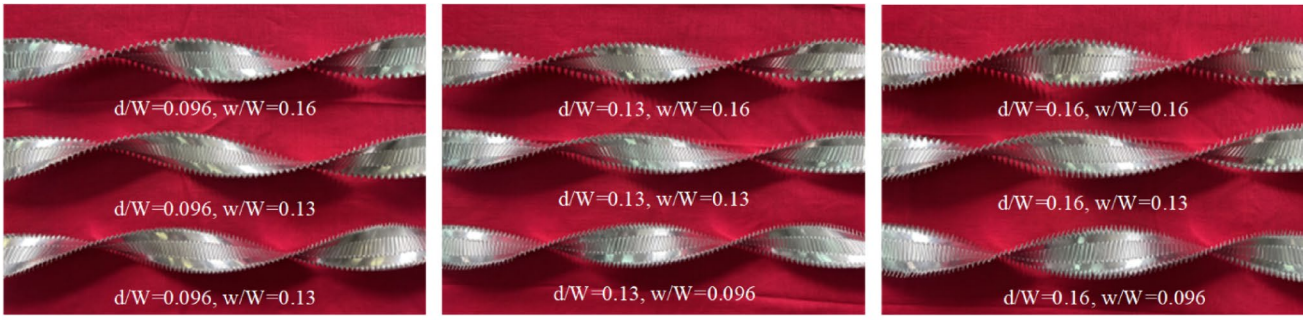

(a) picture view

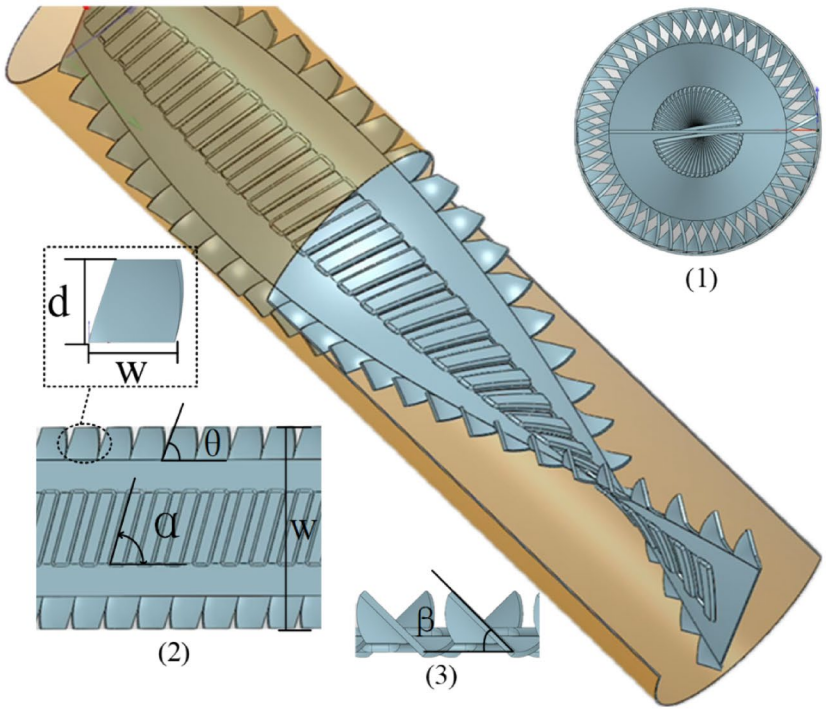

(b) model of I-RTTW

Fig. 2. Details of I-rib twisted tape and twisted winglets (I-RTTW): (**a**) Top view of I-RTTW; (**b**): (1) Side View; (2) Cut winglet dimensions wing width (*w*) wing length (d), I-type rib angle(α); (3) Twist the winglet angle(β). (**a**) picture view, (**b**) model of I-RTTW.

The preparation process of an I-RTTW is shown in Fig. 3. First, a continuous I-rib structure is formed in the central area of a rectangular aluminum plate (original size, 1200 mm×62 mm×0.8 mm) by mechanical pressing. The rib body and edge of the plate are inclined at an $\alpha = 75°$ angle. Then, the prefabricated plate is placed in a torsion forming device and subjected to an overall spiral twist ratio (y/W) of 4.0. After twisting, cutting is performed along the edge of the plate, and the angle between the cut blade and the edge is controlled at $\theta = 75°$ to form regularly arranged edge winglets. Finally, each winglet is subjected to a local twist of $\beta = 45°$ to construct a microscale vortex-inducing structure. The geometric parameters of the winglets include winglet depth ratios (d/W, the ratio of the winglet expansion depth to the plate width) of 0.096, 0.13, and 0.16, and winglet width ratios (w/W, the ratio of the winglet width to the plate width) of 0.096, 0.13, and 0.16. The enhanced heat transfer mechanism of this composite structure is as follows. The edge winglets induce micro-scale vortices near the tube wall, effectively disrupting boundary layer development and guiding the fluid to the central flow area. Concurrently, the I-type ribs in the central area promote momentum exchange between the wall boundary layer fluid and the core flow area by generating secondary swirl flow, forming a more uniform mixed flow field. This achieves a significant improvement in the convective heat transfer coefficient.

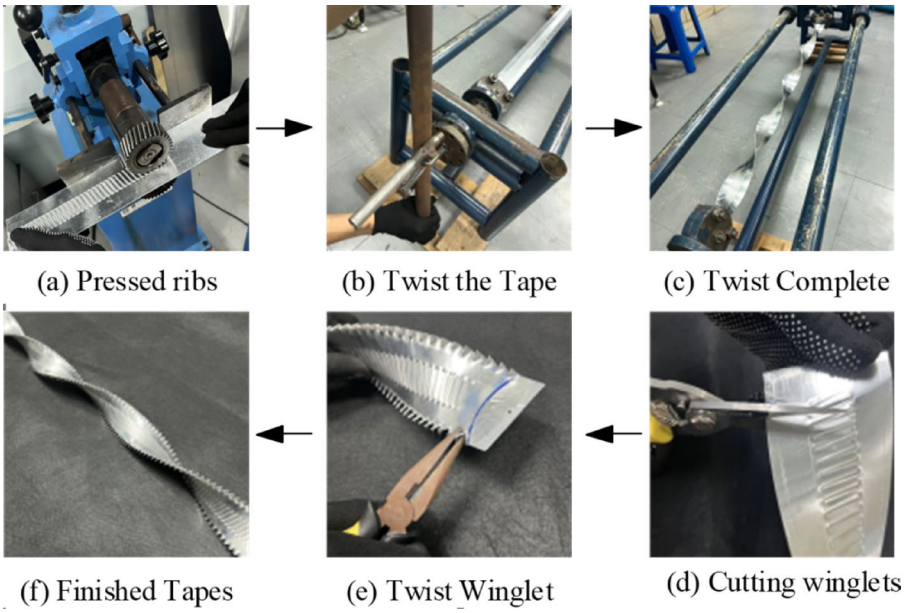

Fig. 3. I-RTTW production process.

Experimental details

As shown in Fig. 4, this experimental system has four parts: a heating section, a flow control section, a temperature and pressure measurement section, and a data acquisition system. In the design of the heating section, a copper tube with an inner diameter of 62 mm, a wall thickness of 2.0 mm, and a length of 1,500 mm is selected as the heating channel. The outer wall of the copper tube is tightly wound with a resistance wire heating element. The heating power is precisely controlled with a variable transformer to create a constant heat flux boundary condition at the tube wall and ensure the stability of the heat load during the experiment. The air source of the flow control section is compressed air. The air flow output by the compressor is adjusted with an orifice flowmeter. Through reasonable control, the experimental working conditions cover the turbulent flow range of Reynolds numbers (*Re*) 6,000 ~ 20,000. Additionally, a rectifier is set at the front end of the heating tube inlet. This can effectively reduce the unevenness of the incoming flow and ensure that the airflow entering the heating section has good stability and uniformity. The temperature and pressure measurement section uses several high-precision sensors to measure temperature and pressure parameters. The arrangement of temperature detection is shown in Fig. 5. T-type thermocouples are used to measure the temperature. The measuring points are arranged at intervals of 100 mm along the axial direction of the heating area. A total of 15 temperature measurement sections are set up to achieve refined measurement of the fluid temperature distribution. A thermal resistance detector (RTD) is installed at the inlet of the heating tube to monitor the inlet temperature, and 4 RTDs are arranged to accurately measure the outlet temperature to obtain complete temperature field information. Pressure measurement is achieved by installing pressure sensors at the inlet and outlet of the heating tube to obtain flow pressure drop data during the experiment. This provided a basis for subsequent flow resistance characteristic analysis. The data acquisition system consists of a data acquisition card and a computer, which work together to achieve real-time synchronous acquisition of experimental temperature and pressure data. The system has the characteristics of high precision and stability, which can effectively ensure the accuracy and integrity of experimental data and provide dependable support for subsequent experimental data analysis.

The new enhanced heat transfer element is a twisted tape with pressed I- Ribs on the surface. It is made of 0.8 mm-thick aluminum sheet and has a width consistent with the inner diameter of the heating tube (62 mm). The edge of the twisted tape is designed with a cutting winglet having a torsion angle of 45°. During installation, it is fixed by tightly fitting the inner wall of the tube to ensure that there is no significant gap between the tube wall and avoid fluid leakage and flow state interference. The twist ratio of the twisted tape is set to 4.0 to explore the heat transfer enhancement effect under this structural parameter. During the experiments, the heat flux of the tube is maintained, and the Reynolds number is changed by adjusting the air flow rate. The heat transfer and flow resistance characteristics of this new twisted tape under turbulent flow conditions are systematically studied.

Data summary

Comparison of experimental data with correlation

First, the Nusselt numbers and friction coefficients for the plain tube in this study were evaluated against standard correlations for validation. The Dittus–Boelter, Gnielinski, and Blasius correlations[35] were employed as reference standards.

The Dittus-Boelter correlation is:

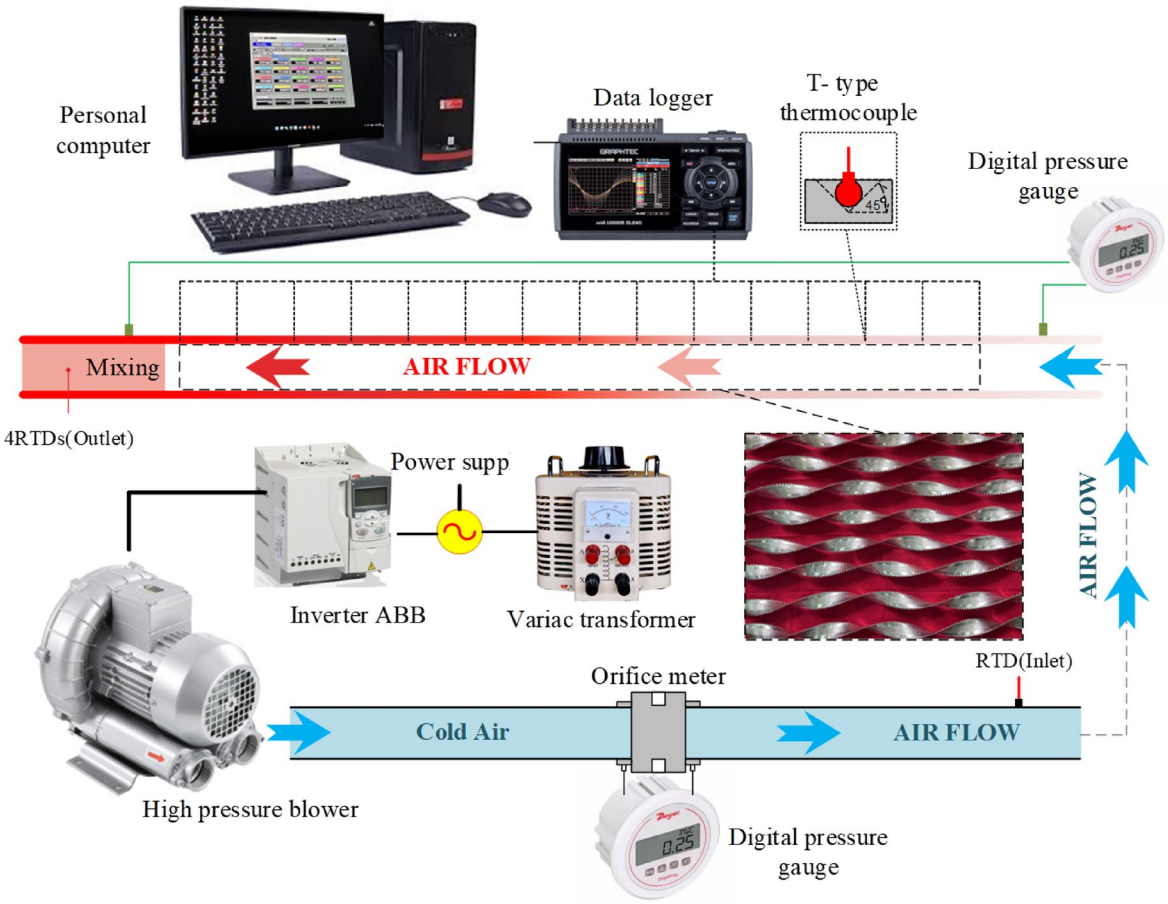

Fig. 4. Schematic diagram of the experimental equipment.

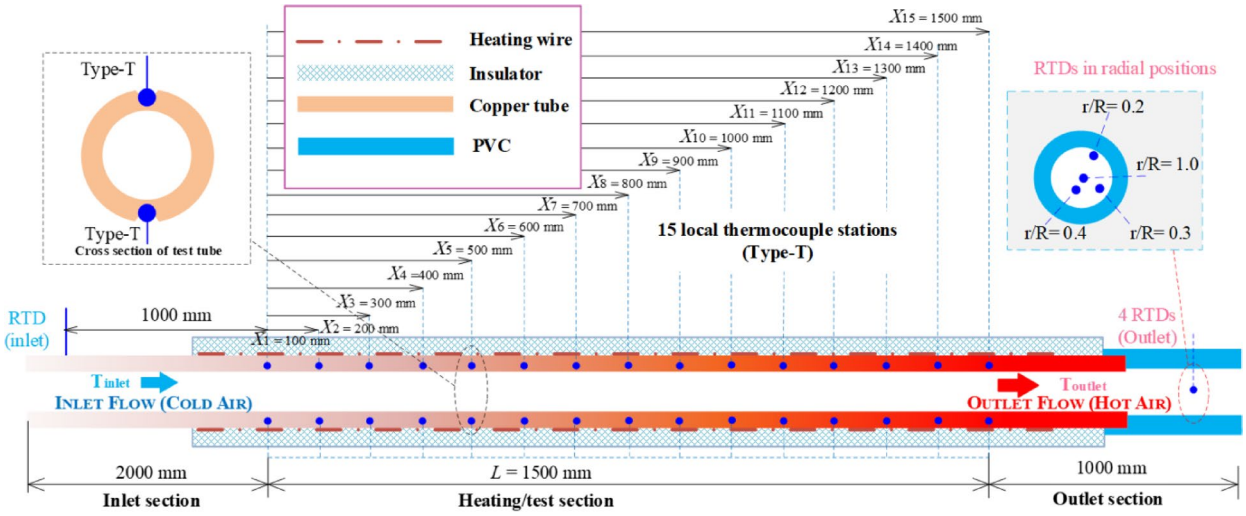

Fig. 5. Schematic diagram of the temperature measurement section.

$$Nu = 0.023Re^{0.8}Pr^{0.4} \tag{1}$$

where the validity of *Pr* and *Re* is $0.6 \ll Pr \ll 160, \quad Re > 10,000.$

The Gnielinski correlation is:

$$Nu = \frac{(f/8)(Re-1{,}000)Pr}{1+12.7\left(\frac{f}{8}\right)^{\frac{1}{2}}\left(Pr^{\frac{2}{3}}-1\right)} \tag{2}$$

where the validity of *Pr* and *Re* is $0.5 \ll Pr \ll 2000, \ 3,000 \ll Re \ll 5 \times 10^6$ and *f* is the Darcy friction factor.

The Blasius equation for turbulent flow in tubes for $3,000 \ll Re \ll 5 \times 10^4$is:

$$f = 0.316Re^{-0.25} \tag{3}$$

The comparison in Fig. 6(a) shows that within the full range of measured Reynolds numbers, the maximum deviations of the experimental Nusselt number data from the Dittus-Boelter and the Gnielinski equations are 9.82% and 6.61%, respectively. Figure 6(b) compares the experimentally measured friction coefficients with those calculated using the Blasius formula. The results show a maximum deviation of 1.21%, with all errors remaining below 10%, demonstrating the reliability of the experimental setup and the accuracy of the measurements.

Experimental calculations

In the experiments, the inner wall of the heating tube was set to a constant heat flux boundary condition. The inlet air temperature (T_i) was maintained at 25 °C. Heat generated by the heating wire was conducted to the inner surface through the tube wall, and then transferred to the air flowing in the tube by convection. Based on the principle of energy conservation, the heat absorbed by the air (Q_{air}) is equal to the heat transferred by wall convection (Q_{conv}), satisfying the thermal equilibrium relationship.

$$Q_{air} = Q_{conv} \tag{4}$$

where Q_{air} is:

$$Q_{air} = \dot{m}C_{p,air}\left(T_o - T_i\right) \tag{5}$$

The internal convection thermal performance is determined using the average heat gain in the air:

$$Q_{conv} = hA\left(\widetilde{T}_W - T_b\right) \tag{6}$$

where T_b is the average temperature of the bulk flow:

$$T_b = \frac{T_o+T_i}{2} \tag{7}$$

The average surface temperature (T_w) is determined by measuring the temperature data between the system inlet and outlet using thermocouple probes as:

$$T_w = \sum \frac{T_w}{15} \tag{8}$$

The convective heat transfer coefficient (*h*) between the air and the test tube wall is defined as:

$$h = \frac{\dot{m}C_{p,air}(T_o-T_i)}{A\left(\widetilde{T}_W-T_b\right)} \tag{9}$$

where *A* is the inner surface area of heat transfer and is determined by:

$$A = \pi\, DL \tag{10}$$

in which *D* is inner diameter of the test tube.

The Nusselt number (*Nu*) is determined by:

$$Nu = \frac{hD}{k} \tag{11}$$

where *k* is the air heat conduction coefficient.

μ represents the viscosity of air. Calculation of the Reynolds number in a circular tube is as follows:

$$Re = \frac{\rho\, UD}{\mu} \tag{12}$$

The friction coefficient (*f*) is calculated from the experimentally measured pressure drop data:

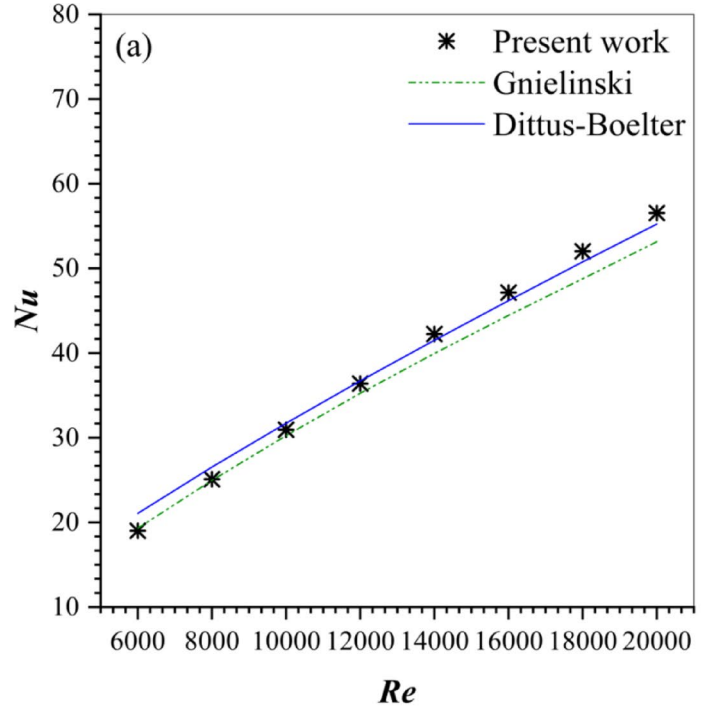

(a)

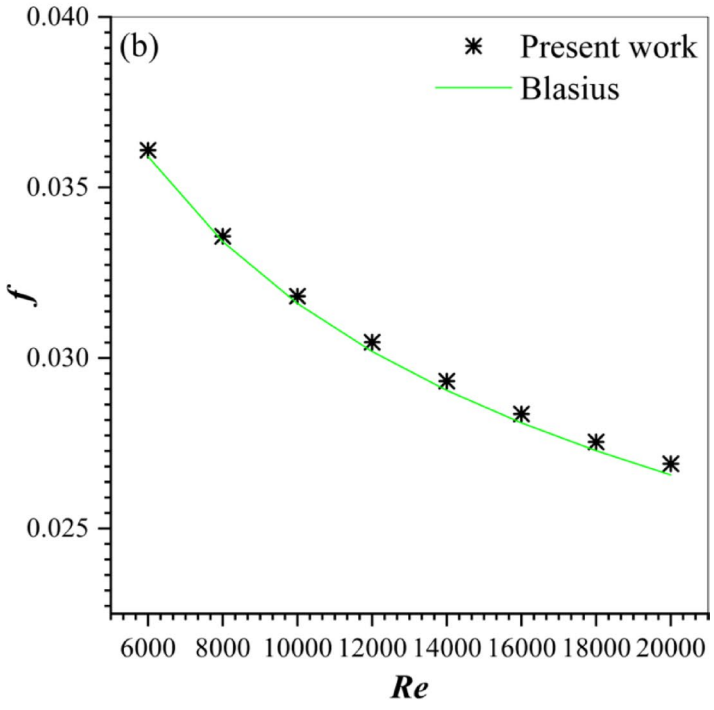

(b)

Fig. 6. Correlation between plain tube experimental data and standards: (**a**) *Nu* and (**b**) *f*.

$$f = \frac{\Delta P}{\left(\frac{L}{D}\right)\left(\rho \frac{U^2}{2}\right)} \tag{13}$$

In thermal performance evaluation, the constant pumping power is usually used as a constraint and expressed as TPI[33,34], which is calculated as follows:

$$\dot{V}_p \Delta P_p = \dot{V}_t \Delta P_t \tag{14}$$

Where $\dot{V}_p$ and $\dot{V}_t$ represent the volume flow rate through the tube; $\Delta P_p$is the pressure drop without turbulators, and ΔP_t is the pressure drop with twisted tapes. Using the Darcy equation to calculate the pressure drop and the Reynolds number (Re) under various geometric shapes, the pumping power is proportional to fRe^3, and Eq. (14) can be rewritten as:

$$f_p Re_p^3 = f_t Re_t^3 \tag{15}$$

It is generally accepted in the literature that the friction coefficient of both pipes and pipes with turbulators is related to the Reynolds number and follows the following equation:

$$f = aRe^b \tag{16}$$

Under the constraint of constant pumping power, there must be a difference in the mass flow rate (or Reynolds number) flowing through the internal enhanced channel and the reference plain tube. This is because, to maintain a constant fluid pumping power, the mass flow rate in the smooth channel needs to be increased. Based on this, using Eqs. (15) and (16), the Reynolds number Re_p of the smooth tube can be expressed as:

$$Re_p = \left(\frac{a_t}{a_p}\right)^{\frac{1}{3+b_p}} Re_t^{\frac{3+b_t}{3+b_p}} \tag{17}$$

The correlation formula of Nu_p and f_p obtained from the present plain tube in this experiment is as follows[35,36]:

$$Nu_p = 0.0027 Re_p^{1.031} Pr^{0.4} \tag{18}$$

$$f_p = 0.3023 Re_p^{-0.244} \tag{19}$$

Combining Eqs. (15), (19) and (24), the Reynolds number (Re_p) of a plain tube can be expressed as a function of the Reynolds number (Re_t) of the I-RTTW:

$$Re_p = 2.846 Re_t^{0.965} (d/W)^{0.081} (w/W)^{0.047} \tag{20}$$

Under constant pump power conditions, the thermal performance index can be expressed as:

$$TPI = \frac{h_t}{h_p} = \frac{Nu_t}{Nu_p} \tag{21}$$

Combining Eqs. (18), (23), (20) and (21), the heat transfer efficiency expression of the I-RTTW turbulator can be obtained:

$$TPI = 5.8 Re_t^{-0.156} (d/W)^{0.0804} (w/W)^{0.0428} \tag{22}$$

Uncertainty calculation

To ensure the reliability of the experimental results, an uncertainty analysis was performed for key parameters, including the Reynolds number (Re), Nusselt number (Nu), and friction factor (f). Since both Nu and pressure drop measurements inherently contain some degree of uncertainty, the ranges were determined in strict accordance with established guidelines[37,38]. Table 1 presents a comprehensive summary of uncertainties for all test parameters, serving as a clear reference for interpreting the results and verifying the findings.

Variables	(%) Uncertainties device/Method used
Kinematic viscosity, μ	± 2.11 Curve-fitting formula
Differential pressure, ΔP	± 1.3 Dwyer MS2
Air velocity, U	± 2.41 Hot-wire Anemometer
Thermal conductivity, k	± 3.1 Curve-fitting formula
Air temperature, T	± 0.1 RTD Pt100
Density, ρ	± 2.17 Curve-fitting formula
Power input	± 0.5% Digital Power Meter

Table 1. Specifications of experimental uncertainties.

Throughout all test runs, the I-RTTW twist ratio was kept constant at 4.0. The twist ratio (*y*/*W*) is defined as the axial distance between two corresponding points on a coplanar surface perpendicular to the tape axis when the tape is twisted by 180°, divided by the tape width. This dimensionless parameter characterizes the geometric configuration of the twisted tape.

Nusselt Number (*Nu*)

$$\begin{aligned}\frac{\Delta Nu}{Nu} &= \frac{1}{Nu}\left[\left\{\frac{\partial}{\partial h}(Nu)\,\Delta h\right\}^2+\left\{\frac{\partial}{\partial D}(Nu)\,\Delta D\right\}^2+\left\{\frac{\partial}{\partial k}(Nu)\,\Delta k_a\right\}^2\right]^{0.5}\\ &= \left\{\left(\frac{\Delta h}{h}\right)^2+\left(\frac{\Delta D}{D}\right)\right\}^{0.5}\end{aligned} \tag{23}$$

Where $h=\frac{q''}{T_\omega - T_b}$.

$$\begin{aligned}\frac{\Delta h}{h} &= \frac{1}{h}\left[\left\{\frac{\partial h}{\partial q''}\Delta q''\right\}^2+\left\{\frac{\partial h}{\partial T_\omega}\Delta T_\omega\right\}^2+\left\{\frac{\partial h}{\partial T_b}\Delta T_\omega\right\}^2\right]^{0.5}\\ &= \left[\left\{\frac{\Delta q''}{q''}\right\}^2+\left\{\frac{\Delta T_\omega}{T_\omega - T_b}\right\}^2+\left\{\frac{\Delta T_b}{T_\omega - T_b}\right\}^2\right]^{0.5}\end{aligned} \tag{24}$$

Where $q''=\frac{0.5}{\pi DL}\left[\left(V^2/R\right)+\dot{m}C_p\left(T_o-T_i\right)\right]$ . .

Friction factor (*f*).

$$\begin{aligned}\frac{\Delta f}{f} &= \frac{1}{f}\left[\left\{\frac{\partial f}{\partial(\Delta P)}\Delta(\Delta P)\right\}^2+\left\{\frac{\partial f}{\partial L}\Delta L\right\}^2+\left\{\frac{\partial f}{\partial D}\Delta D\right\}^2+\left\{\frac{\partial f}{\partial Re}\Delta Re\right\}^2\right]^{0.5}\\ &= \left[\left\{\frac{\Delta(\Delta P)}{\Delta P}\right\}^2+\left\{\frac{\Delta L}{L}\right\}^2+\left\{\frac{3\Delta D}{D}\right\}^2+\left\{\frac{2\Delta Re}{Re}\right\}^2\right]^{0.5}\end{aligned} \tag{25}$$

Where $\frac{\Delta(\Delta P)}{\Delta P}=\frac{\Delta h}{h}$ and $\frac{\Delta Re}{Re}=\left[\left(\frac{\Delta \dot{m}}{\dot{m}}\right)^2+\left(\frac{\Delta D}{D}\right)^2\right]^{0.5}$.

The variability for *Re*, *Nu*, and *f*, were ± 3.39%, ± 3.46%, and ± 5.12%, respectively.

Mathematical model and numerical method

Procedure for resolution

In this study, the finite volume method is used to carry out three-dimensional numerical simulation of the periodic flow and thermal characteristics of incompressible air in a circular tube equipped with a continuous I-rib twisted tape and twisted winglets (I-RTTW). In order to clarify the research boundaries and simplify the analysis process, the following basic assumptions are made: (1) the flow state is steady and the fluid is incompressible; (2) the flow form of the fluid flowing through the I-RTTW is turbulent; (3) the effects of natural convection and thermal radiation on the flow and heat transfer process are ignored; (4) the thermophysical properties of the fluid do not change with temperature. Based on the above assumptions, this study constructs a set of governing differential equations to describe the flow and heat transfer behavior of the fluid in a circular tube equipped with an I-RTTW. The flow and heat transfer phenomena are jointly governed by the steady-state three-dimensional forms of the continuity equation, momentum equation, and energy equation. In the numerical calculation process, the computational domain is discretized using conventional Cartesian grid cells. For the steady-state flow case, the time-averaged incompressible Navier-Stokes equations expressed in Cartesian tensor notation can be expressed as follows:

Continuity equation:

$$\frac{\partial}{\partial x_i}(\rho u_i)=0 \tag{26}$$

Momentum equation:

$$\frac{\partial\left(\rho u_i u_j\right)}{\partial x_i}=-\frac{\partial p}{\partial x_i}+\frac{\partial}{\partial x_j}\left[\mu\left(\frac{\partial u_i}{\partial x_j}+\frac{\partial u_j}{\partial x_i}-\frac{2}{3}\delta_{ij}\frac{\partial u_k}{\partial x_k}\right)\right]+\frac{\partial}{\partial x_j}\left(-\rho\,\overline{u_i' u_j'}\right) \tag{27}$$

Energy equation:

$$\frac{\partial}{\partial x_i}\left[u_i(\rho E+p)\right]=\frac{\partial}{\partial x_j}\left(k_{eff}\frac{\partial T}{\partial x_j}\right),\ E=h-\frac{p}{\rho}+\frac{u^2}{2} \tag{28}$$

Furthermore, an enhanced wall treatment model was selected for near-wall modeling. Its key advantage lies in its ability to adapt to the fine near-wall mesh required for resolving the viscous sublayer, thus laying the foundation for accurate simulation of the near-wall flow field. To optimize the I-RTTW mesh size, the Richardson

extrapolation technique was used to verify mesh independence for computational meshes with varying mesh sizes. During the meshing process, GAMBIT 2.1 software was used to generate triangular meshes for the pipe wall and insert surfaces. Local mesh refinement was performed in the boundary layer region, and adaptive mesh refinement was also performed during the preliminary calculation phase to ensure mesh accuracy in critical areas. The mesh independence scheme was evaluated by comparing the results at different mesh levels (using the Nusselt number and friction factor as key indicators).

Periodic boundary conditions were applied to the inlet and outlet boundaries of the flow domain, and the velocity profiles were consistent. To simplify the calculations, the physical properties of the air were assumed to be constant at the bulk average temperature. Impermeable boundary conditions and no-slip wall conditions were applied to the surface and walls of tube I-RTTW. Notably, the dimensionless temperatures at the inlet and outlet were identical. The time-independent, incompressible Navier-Stokes equations were discretized using the finite volume method. The convection terms were discretized using QUICK (a convective dynamics difference scheme with quadratic upstream interpolation), while the diffusion terms were discretized using a central difference scheme. The discretized nonlinear equations were solved implicitly, and the pressure field was calculated using SIMPLE (a semi-implicit method for pressure-velocity coupling). A fully developed velocity profile was applied at the inlet boundary, along with an impermeable boundary condition. Unless otherwise specified, the turbulence intensity at the inlet was fixed at 10%. In this study, the RNG k-ε model was used to simulate the turbulent flow regime. The calculation continues until the normalized residuals of the algebraic equations meet the convergence criteria by a predetermined value—specifically, the residual of the energy equation must be less than 10^{-9}, and the residuals of all other variables must be less than 10^{-5}. Based on the inlet conditions, a Reynolds number of 10,000 was used in this calculation.

Numerical calculation results

To better understand the effect of the number of I-RTTW on heat transfer and friction loss characteristics, Figs. 7, 8, 9 and 10 present streamlines, velocity vectors, turbulent kinetic energy (TKE), fluid temperature, and Nusselt number distribution (Nu) at a Reynolds number of 10,000. The streamline contours in Fig. 7 clearly demonstrate that the shearing effect of the winglet on the fluid causes significant flow separation and reattachment as the fluid flows over the winglet. Notably, this reattachment process induces longitudinal vortices in the wall region, which effectively destabilize the boundary layer and enhance heat transfer. Further observation reveals that the flow rate between the winglets increases significantly when the winglet depth-to-width ratio is at its maximum. This increase in flow significantly enhances the perturbation of the boundary layer, doubling the degree of boundary layer disruption. Consequently, this parameter combination significantly improves heat transfer.

Figure 8 shows the distribution of turbulence kinetic energy (TKE) and flow field vectors across the duct cross section for different relative winglet sizes (w/W and d/W). Colors from blue to red represent low to high turbulence intensity, and arrows represent local velocity vectors. As the winglet size increases, the distribution characteristics of the turbulence kinetic energy and its impact on fluid heat transfer show significant changes. Under the conditions of $w/W = 0.096$ and $d/W = 0.096$, the high turbulence kinetic energy region is primarily concentrated near the turbulent element, while the core and some near-wall regions maintain relatively low turbulence levels, indicating that the disturbance has limited impact on radial mixing. At this condition, radial heat transfer is slow, the thermal boundary layer is less disrupted, and the improvement in convective heat transfer is relatively small. When the size increases to $w/W = 0.13$ and $d/W = 0.13$, the high turbulence region significantly expands, the vortex coverage increases, and the secondary flow intensity increases, resulting in more efficient heat exchange between the core flow and the near-wall flow. The thickness of the thermal boundary layer decreases, effectively weakening the radial temperature gradient, significantly improving heat transfer efficiency. Under the conditions of $w/W = 0.16$ and $d/W = 0.16$, the turbulent kinetic energy reaches its highest level, the high turbulence region covers almost the entire cross-section, the vortex structure is strong, and the disturbance near the wall is particularly significant. The thermal boundary layer is extensively destroyed, and the heat transfer capacity reaches its peak. At this point, the secondary flow structure is significantly enhanced, the exchange between the core flow and the near-wall flow becomes more frequent, and the radial mixing effect is greatly improved. The strong near-wall turbulence effectively weakens the thermal boundary layer, reduces the radial temperature gradient, and significantly enhances the heat transfer process. The high turbulent kinetic energy and strong secondary flow work together to promote rapid and frequent heat exchange between the high-temperature fluid in the core area and the low-temperature fluid on the wall. The thickness of the thermal boundary layer is significantly reduced, and the local heat transfer coefficient is significantly improved.

The combined temperature field (Fig. 9) and the surface Nusselt number distribution (Fig. 10) show that with increasing the I-RTTW geometric parameters w/W and d/W, the flow disturbance and turbulence within the pipe significantly increase, the local Nusselt number on the wall improves overall, and the high heat transfer region (red stripe area) expands in both area and intensity, indicating that the overall convective heat transfer capacity is enhanced. However, increasing the I-RTTW geometric parameters also leads to increased temperature field non-uniformity, with the low-velocity recirculation zone and central cold zone behind the torsional band expanding. These areas experience slow fluid turnover and weak convective heat transfer, relying primarily on conductive heat transfer, resulting in distinct low-temperature and low Nu regions. High Nu stripes spatially correspond to regions with large temperature gradients, indicating that vortex scouring of the wall is the primary mechanism for local heat transfer enhancement; the low Nu regions between the stripes correspond to areas of relatively smooth flow. Overall, $d/W = 0.096$, $w/W = 0.096$ maintained good temperature uniformity, but the heat transfer enhancement was limited; $d/W = 0.13$, $w/W = 0.13$ achieved a good balance between enhancing heat transfer and maintaining uniformity; and $d/W = 0.16$, $w/W = 0.16$ achieved the highest heat transfer enhancement.

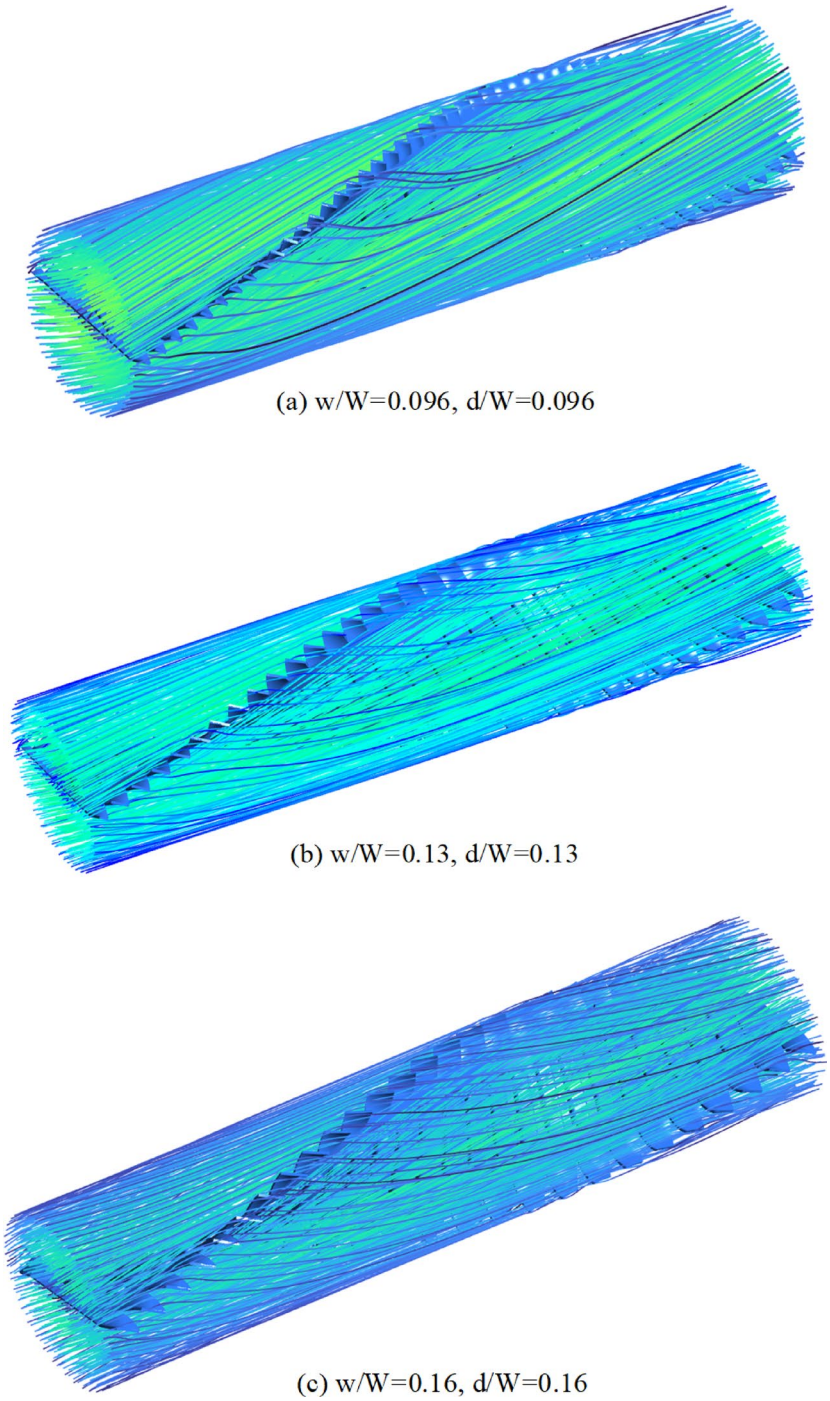

Fig. 7. Streamline cloud diagrams under different wing width ratios and wing depth ratios.

Experimental results

Effect of cutting winglets on heat transfer

Introduction of cut winglets can significantly improve heat transfer of a pipe by disrupting the laminar boundary layer at the tube wall. The enhancement is related to the winglet depth ratio and winglet width ratio parameters.

Effect of wing depth ratio (d/W)

At a fixed wing width ratio, a larger wing depth ratio can achieve better heat transfer. As shown in Figs. 11(a-b), when the wing depth ratio increases from (*d/W*) 0.096 to 0.16 with a 0.16 wing width ratio (*w/W*), the heat transfer rate increases from 177 to 199% that of a plain tube, and from 112 to 126% compared with a typical tape. Under a 0.13 wing width ratio (*w/W*), the heat transfer rate in the corresponding wing depth ratio (*d/W*) range increases from 172 to 195% (plain tube), and 109–124% (TT). With a 0.096 wing width ratio (*w/W*), the

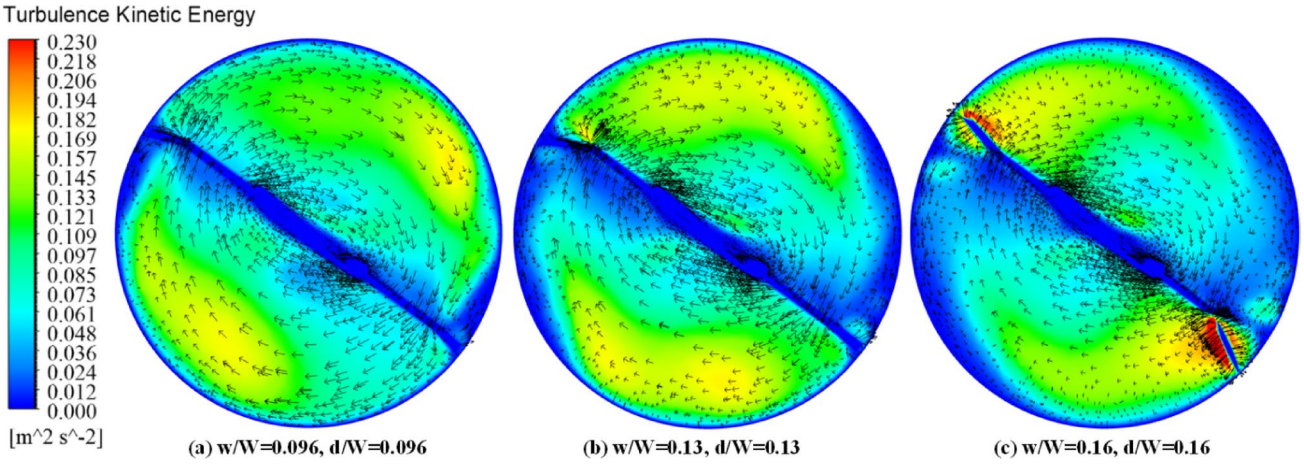

Fig. 8. Effect of flow field and turbulent kinetic energy on I-RTTW at $Re = 10{,}000$.

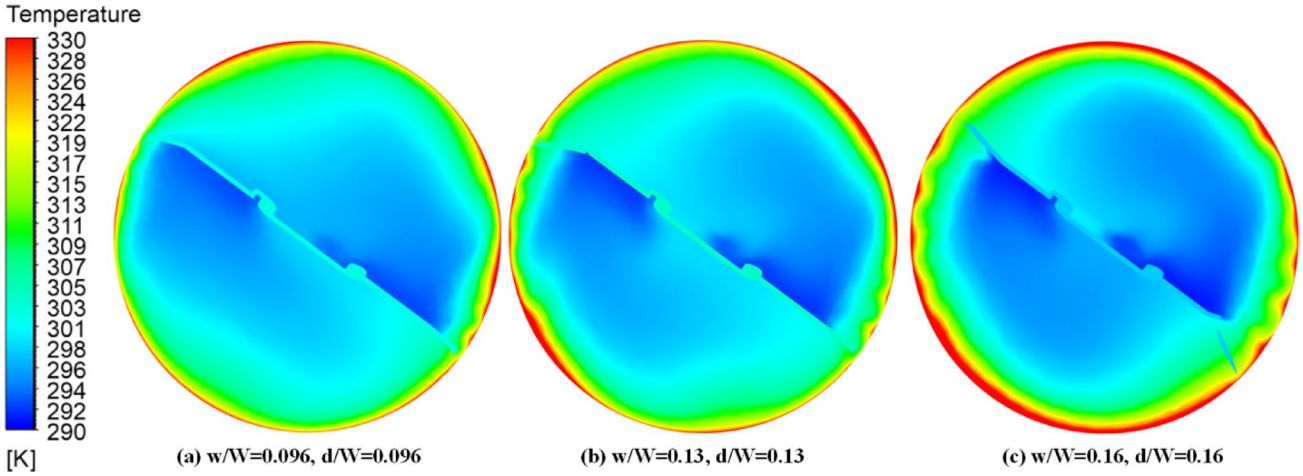

Fig. 9. The influence of I-RTTW on the temperature field at $Re = 10{,}000$.

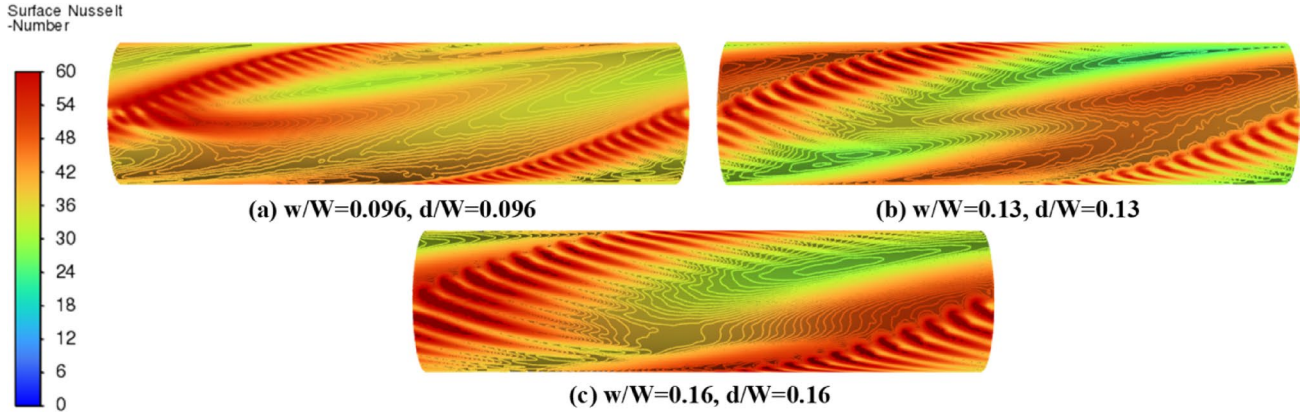

Fig. 10. Effect of the local Nusselt number for I-RTTW at $Re = 10{,}000$.

heat transfer rate in the corresponding wing depth ratio range increases from 168 to 185% (plain tube) and 107–115% (TT). The increased wing depth ratio (d/W) means that the longitudinal size of the cutting winglet increases, which can disturb the fluid more deeply and aggravate the boundary layer. In addition, an increased wing depth ratio (d/W) further intensifies the generation of streamwise vortices. This intensification increases

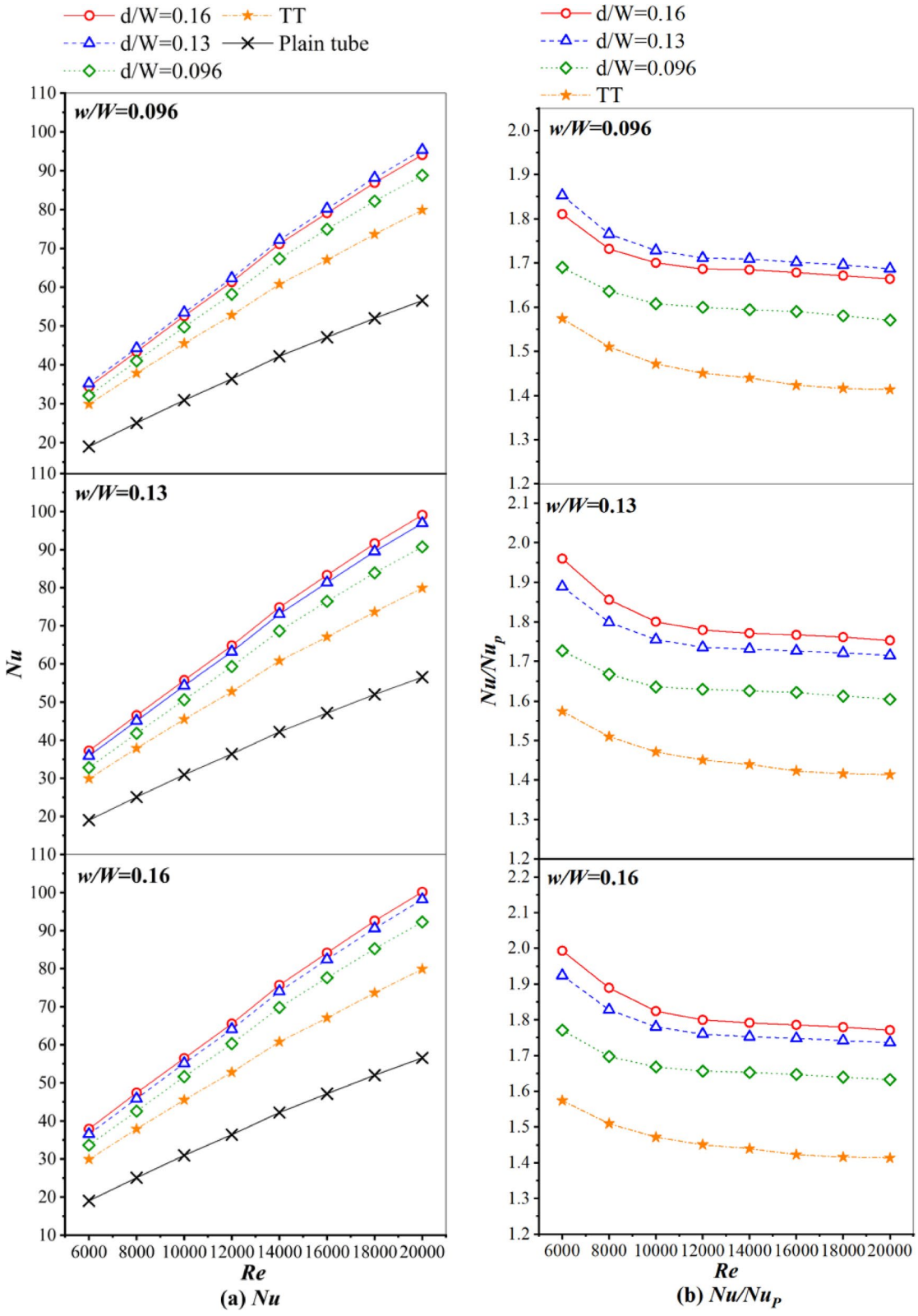

Fig. 11. Effect of I-RTTW on the Nusselt number: (**a**) *Nu* and (**b**) Nu/Nu_p

fluctuations in the near-wall velocity and temperature fields, further disrupting the viscous sublayer. The optimal heat transfer effect is achieved when the wing width ratio (w/W) is 0.16, and the Nusselt number (Nu) is maximal in each group of experiments under this parameter.

Effect of wing width ratio (w/W)
It can be seen from Figs. 12(a-b) that when the wing depth ratio is fixed, a larger wing width ratio improves the mixing efficiency by expanding the fluid movement area. At a wing depth ratio (d/W) of 0.16, when the wing width ratio (w/W) increases from 0.096 to 0.16, the heat transfer rate increases from 181 to 199% compared with a plain tube, and from 115 to 126% compared with a TT. With a wing depth ratio (d/W) of 0.13, the heat transfer rate in the corresponding wing width ratio (w/W) range increases by 185–192% (plain tube) and 117–122% (TT), both of which increase at greater wing width ratios (w/W). At a wing depth ratio (d/W) of 0.096, the heat transfer rate in the corresponding wing width ratio (w/W) range increases by 168–177% (plain tube) and 107–112% (TT), both increasing with greater wing width ratios (w/W). The enhancement mechanisms are closely related to the interaction between the increased winglet span and the boundary layer dynamics. A larger wing width ratio (w/W) extends the disturbance region further along the tube circumference, engaging a greater portion of the near-wall flow. This expanded disturbance region induces stronger cross-stream mixing, which promotes the exchange of fluid from the tube core with fluid in the near-wall region. As a result, the thermal boundary layer is thinned over a larger circumferential area, reducing the overall thermal resistance between the wall and the bulk fluid.

Effect of cutting winglets on the friction factor

The experiments analyze the variation of the friction coefficient of an I-RTTW (I-rib twisted tape and twisted winglet) tube with Reynolds number, revealing the quantitative effects of wing depth ratio (d/W) and wing width ratio (w/W) on fluid resistance characteristics.

Effect of wing depth ratio (d/W)
As shown in Figs. 13(a-b), at a fixed width ratio (w/W), the friction coefficient increases monotonically with the increased wing depth ratio (d/W). When the width ratio (w/W) is 0.16, the friction losses increase from 366 to 412% compared with a plain tube, and from 122 to 137% over that of a TT when the wing depth ratio (d/W) increases from 0.096 to 0.16. At a width ratio (w/W) of 0.13, the increased friction losses in the corresponding wing depth ratio (d/W) range are 356–403% (plain tube) and 119–134% (TT). When the width ratio (w/W) is 0.096, the increased friction losses in the corresponding wing depth ratio range are 346–372% (plain tube) and 115–127% (TT), both of which significantly increase with greater wing depth ratios (w/W). As the wing depth ratio (d/W) increases, the longitudinal size of the cutting wing increases directly, which enhances the disturbance resistance to the fluid, resulting in intensified boundary layer separation, increased eddy loss, and uneven fluid density on the same cross section, causing strong friction loss. Therefore, when the wing depth ratio (d/W) is 0.16, the friction coefficient reaches the experimental maximum value.

Effect of wing width ratio (w/W)
As shown in Figs. 14(a-b), when the wing depth ratio (d/W) is fixed, a larger wing width ratio further increases the friction losses by expanding the fluid action area. When the wing depth ratio (d/W) is 0.16, and the wing width ratio increases (w/W) from 0.096 to 0.16, the friction losses compared with a plain tube increase by 372–412%, and by 124–137% compared to a TT. With a 0.13 wing depth ratio (d/W), the friction losses increase in the corresponding wing width ratio range by 381–394% (plain tube) and 127–131% (TT). At a wing depth ratio (d/W) of 0.096, the friction losses increase over the corresponding wing width ratio range by 346–366% (plain tube) and 115–122% (TT), which generally shows an increase with greater wing width ratios (w/W). The data show that wider winglets produce larger vortices in the radial direction. The increase in radial vortices is accompanied by an increase in flow resistance. The fluid must overcome greater radial shear forces and collision losses, especially when the winglet width ratio reaches 0.16, the friction coefficient reaches the experimental maximum value.

Effect of cutting winglets on the thermal performance index

Effect of wing width ratio (w/W)
A larger wing width ratio can improve heat transfer by expanding the lateral coverage of the wing, enhancing the lateral mixing effect of the fluid, and thereby reducing thermal resistance at the wall. As shown in Fig. 15(a), when the wing depth ratio is fixed, the TPI value increases monotonically at greater wing width ratios. When the wing depth ratio (d/W) is 0.16, the wing width ratio increases from 0.096 to 0.16, and the TPI increases from about 1.03 to 1.29. At high Reynolds numbers ($Re = 20{,}000$), the effect of the wing width ratio tends to be minimal. However, at low Reynolds numbers, wide winglets can more effectively promote mixing, significantly increasing the TPI. The increased wing width ratio (w/W) improves heat transfer by enlarging the mixing area. Although the resistance increases, the greater Nusselt number exceeds the increased friction factor, so the TPI continues to rise. At a 0.16 wing width ratio (d/W), the lateral mixing effect is optimal, and the overall performance is the highest.

Effect of wing depth ratio (d/W)
When the wing depth ratio (d/W) increases, the longitudinal dimension of the wing is greater, which can more deeply disturb the fluid, aggravate boundary layer disruption, and induce stronger secondary flow. This disturbance promotes momentum exchange between the wall fluid and the core flow area, thereby improving heat transfer, but it also increases fluid resistance. As shown in Fig. 15(b), at a fixed wing width ratio (w/W), the

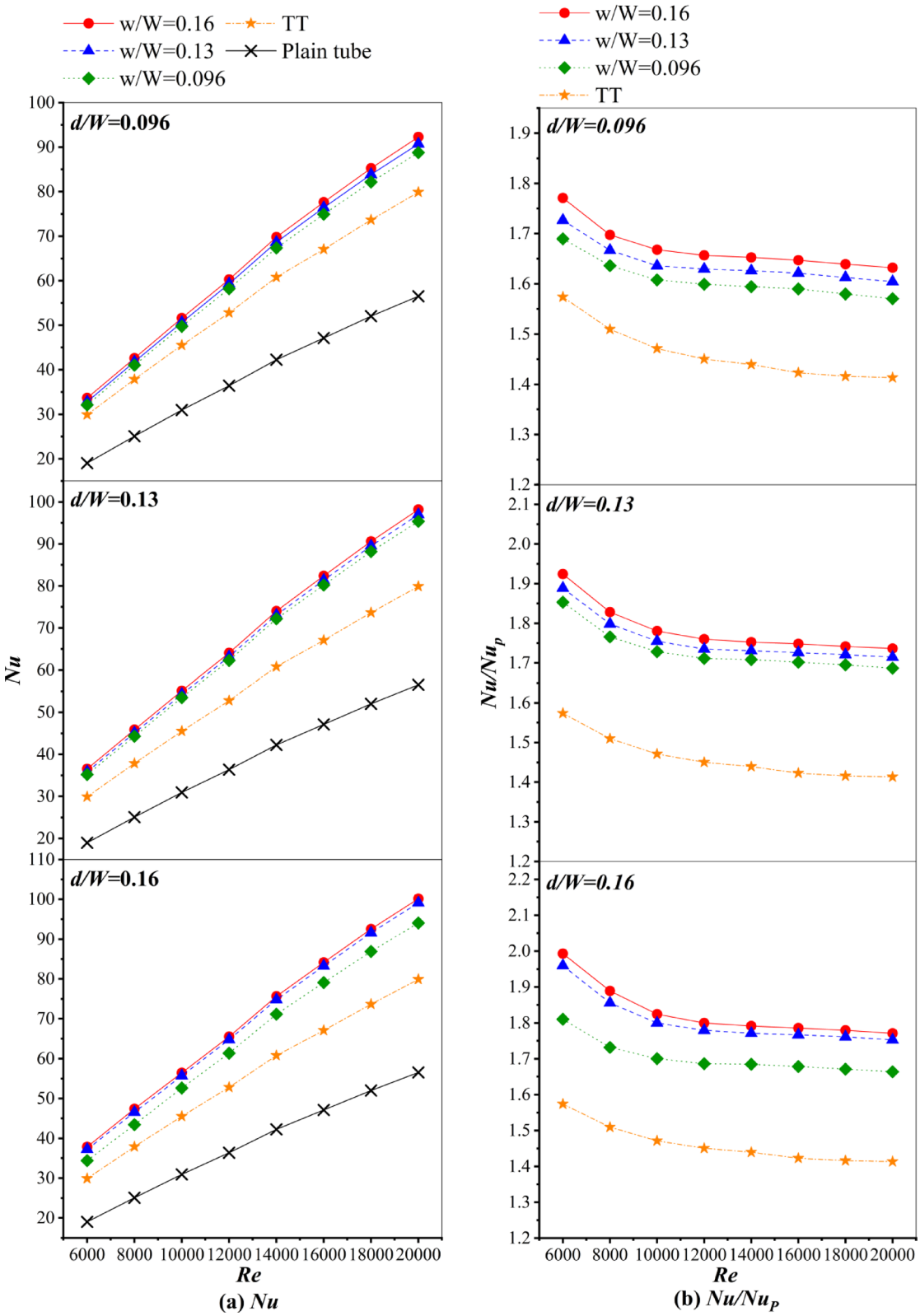

Fig. 12. Effect of I-RTTW on the Nusselt number: (**a**) *Nu* and (**b**) Nu/Nu_p

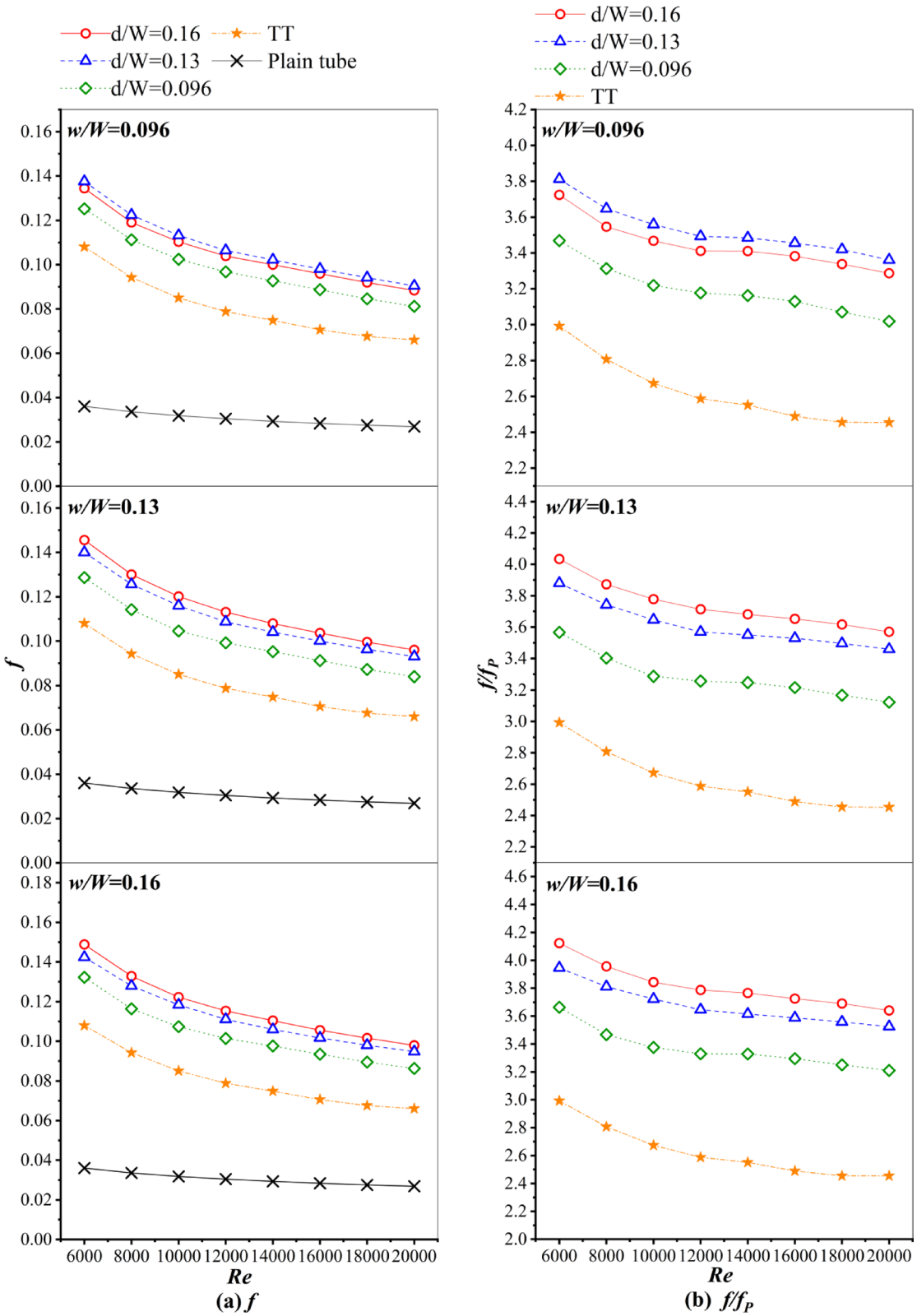

Fig. 13. Effect of I-RTTW on the friction factor: (**a**) *f* and (**b**) *f*/*f*.

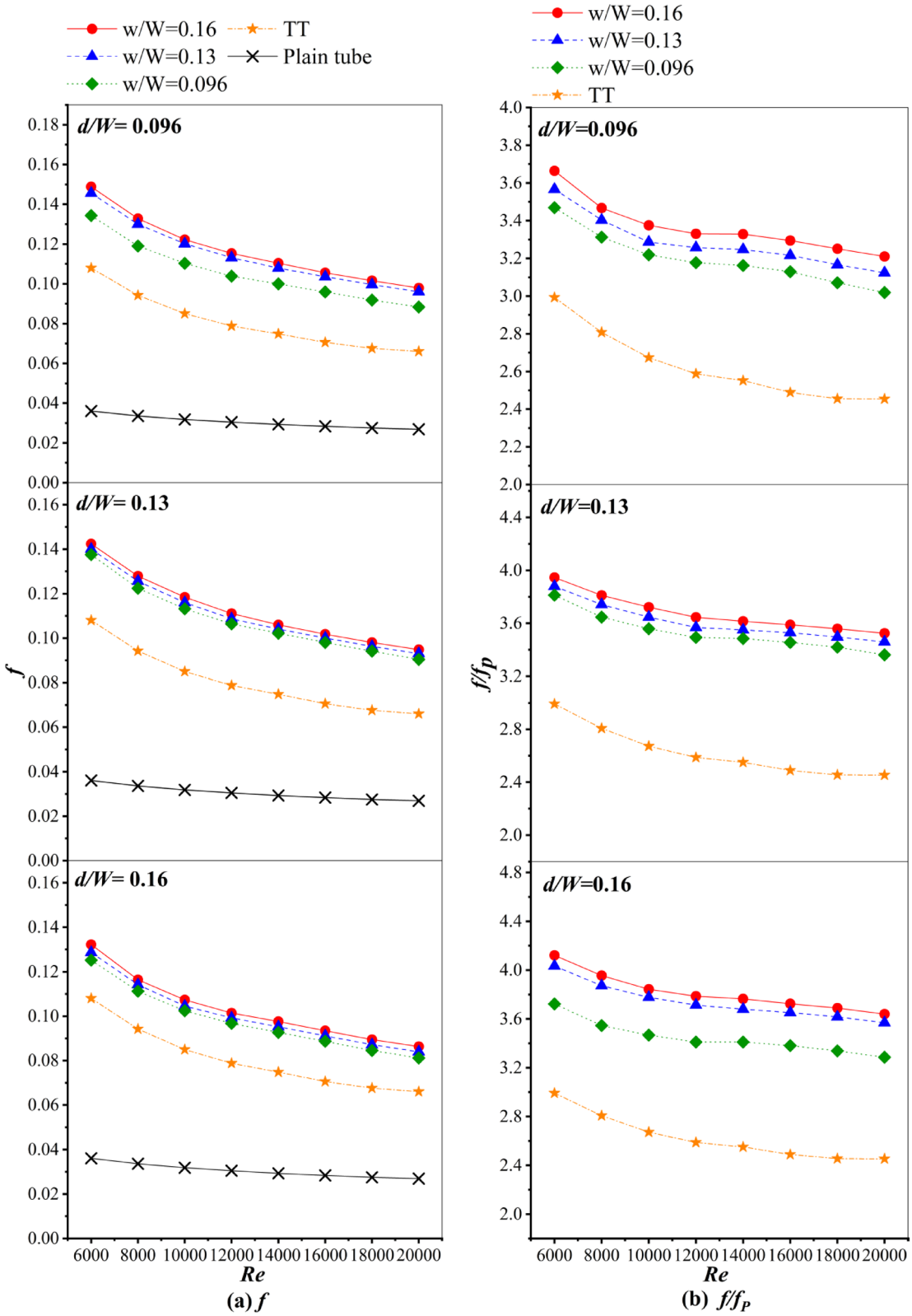

Fig. 14. Effect of I-RTTW on the friction factor: (**a**) *f* and (**b**) *f*/*f*.

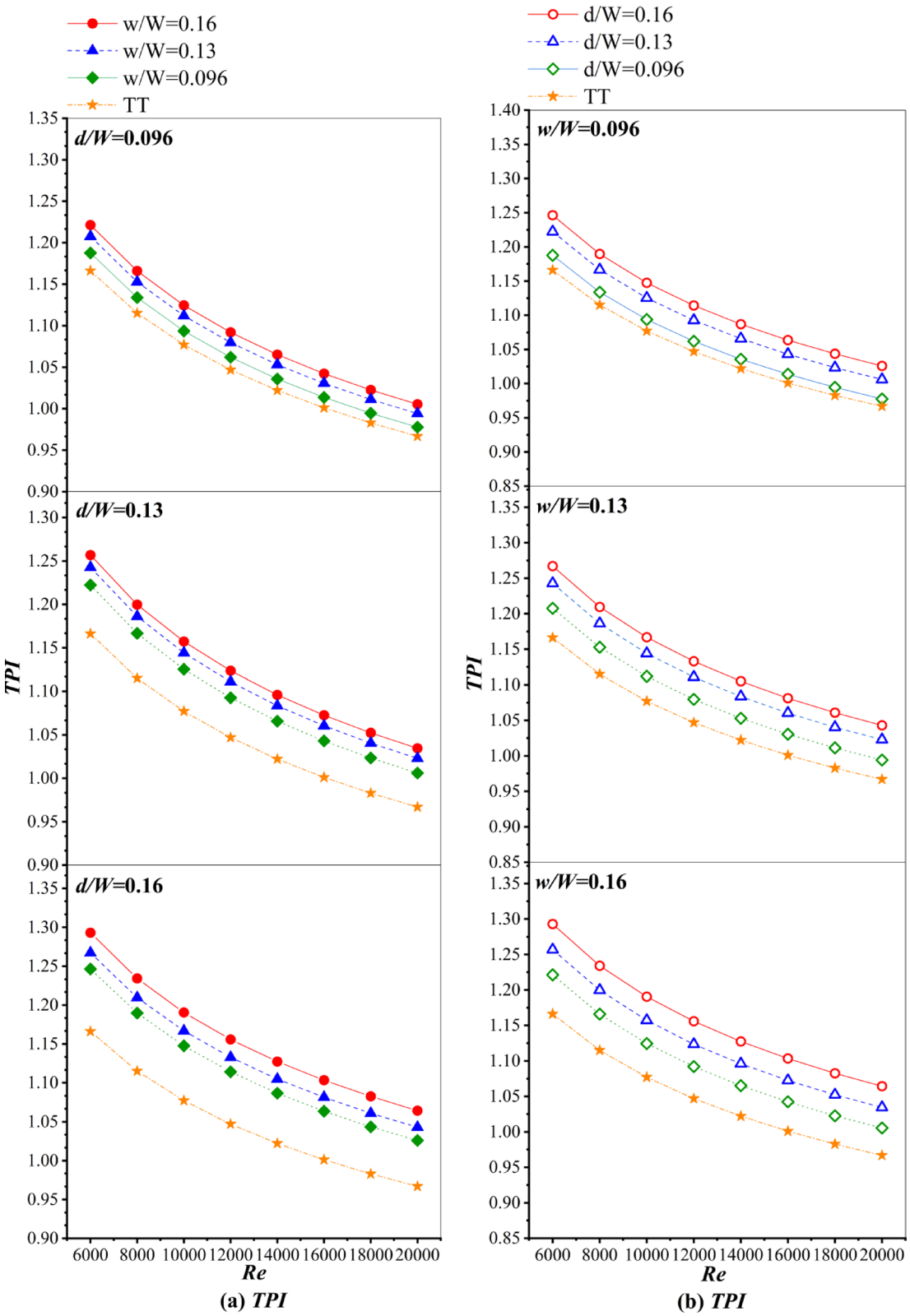

Fig. 15. Effect of I-RTTW on the TPI: (**a**) *w/W* and (**b**) *d/W*.

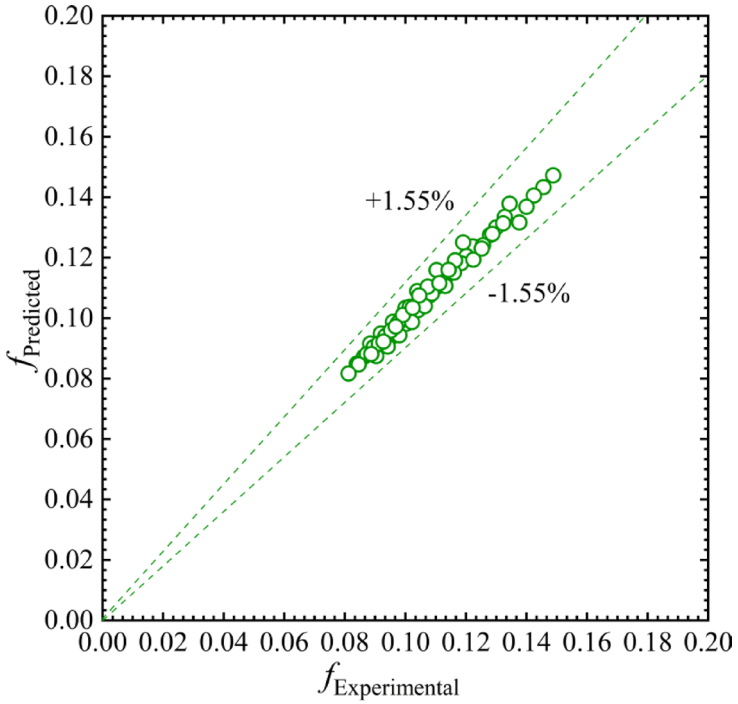

(a) *Nu*

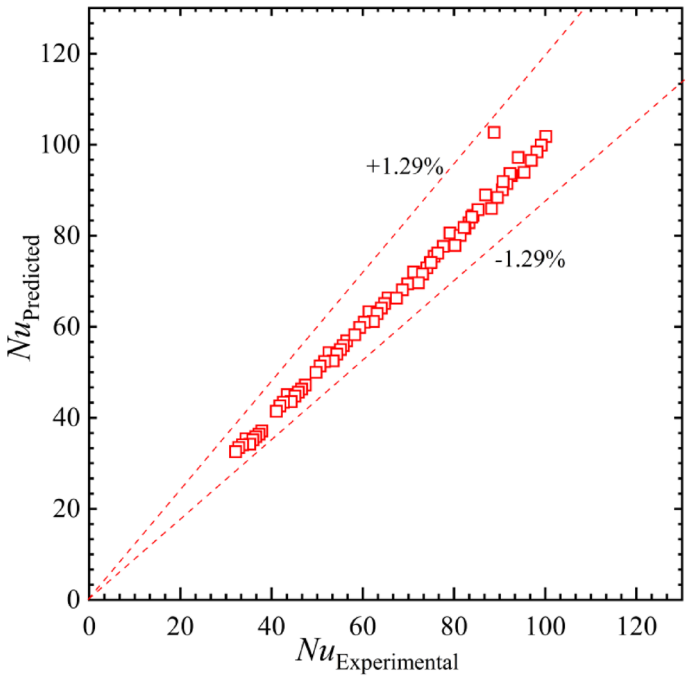

(b) *f*

Fig. 16. Experimental data versus predicted values: (**a**) *Nu*, (**b**) *f*, and (**c**) *TPI*.

TPI value increases monotonically with greater wing depth ratios. At a wing width ratio (*w/W*) of 0.16, the wing depth ratio increases from 0.096 to 0.16, and the TPI increases from 1.0 to 1.29. At low Reynolds numbers (e.g., *Re* = 6,000), the influence of the wing depth ratio is more significant. A larger wing depth ratio can effectively disrupt the boundary layer at low flow rates, resulting in a greater increase in TPI. An increased wing depth ratio has a greater effect on heat transfer than that of increased flow resistance, so the TPI shows an upward trend.

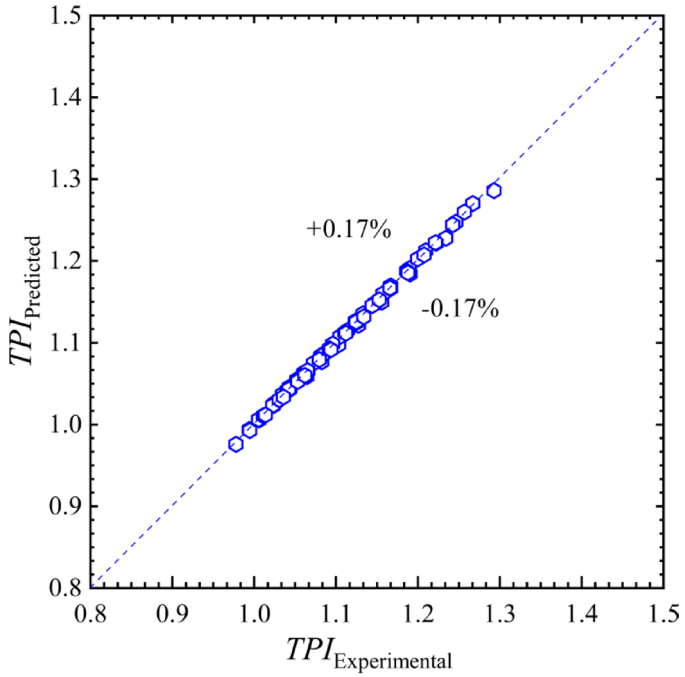

(c) *TPI*

Fig. 16. (continued)

Correlations

This study uses the least squares regression analysis method to systematically construct experimental correlations of Nusselt number (*Nu*), friction coefficient (*f*), and thermal performance index (TPI) for heat exchange tubes equipped with I-rib twisted tapes and twisted winglets (I-RTTW). Using air as a test fluid, experimental research was done under turbulent conditions. The wing depth ratio (*d*/*W*), wing width ratio (*w*/*W*), and Reynolds number (ranging from 6,000 to 20,000) were independent variables. Through in-depth analysis of the experimental data, the following empirical correlations were obtained:

$$Nu = 0.046Re^{0.839}\left(\frac{d}{W}\right)^{0.164}\left(\frac{w}{W}\right)^{0.091}Pr^{0.4} \tag{29}$$

$$f = 5.398Re^{-0.34}\left(\frac{d}{W}\right)^{0.223}\left(\frac{w}{W}\right)^{0.128} \tag{30}$$

$$TPI = 7.03Re^{-0.161}\left(\frac{d}{W}\right)^{0.099}\left(\frac{w}{W}\right)^{0.06} \tag{31}$$

As shown in Fig. 16, this study systematically compares experimentally measured data (Nu_{exp}, f_{exp}, and TPI_{exp}) with the model predictions (Nu_{pred}, f_{pred}, and TPI_{pred}). For the I-rib twisted tape with twisted winglets, the deviations between the experimental and predicted values for Nusselt number (*Nu*), friction coefficient (*f*), and thermal performance index (TPI) are ± 1.29%, ± 1.55%, and ± 0.17%, respectively. Based on the above analysis, these correlations can be used to reliably estimate *Nu*, *f*, and TPI.

Comparison of present data

As shown in Figs. 17 and 18, and 19, the aerodynamic Nu/Nu_p, f/f_p, and thermal performance index (TPI) data of the I-rib twist-tape and twist-tape winglets were compared in this study with those reported in previously published literature [5, 9, 19, 26, 27, 30, and, 40–42]. Under turbulent conditions, the TPI value of the I-RTTW is significantly higher than that of a Sawtooth twisted tape[5], Broken V-ribbed twisted tape[9], Twisted tapes with non-uniform alternate length[19], Serrated wire coil[26], Traverse corrugated tube[27], Tandem wire coil elements[30]. Continuous V-Rib twisted tapes[39], Trapezoidal and twisted trapezoidal tapes[40] and Double V-ribbed twisted-tapes[41].

Figure 17 shows that the Nusselt numbers for the tube with I-rib twisted tape and twisted winglets (I-RTTW) in the present study are significantly higher than those reported in most previous works. Only the serrated wire coil[26], traverse corrugated tube[27], and tandem wire coil elements[30] exhibit comparable Nusselt numbers. Figure 18 indicates that the friction factors in the current study are close to the average of all cases and remain lower than those of the serrated wire coil[26], traverse corrugated tube[27], and tandem wire coil elements[30]. Considering both Nusselt numbers and friction factors, the resulting thermal performance indices (TPI) of the I-RTTW are

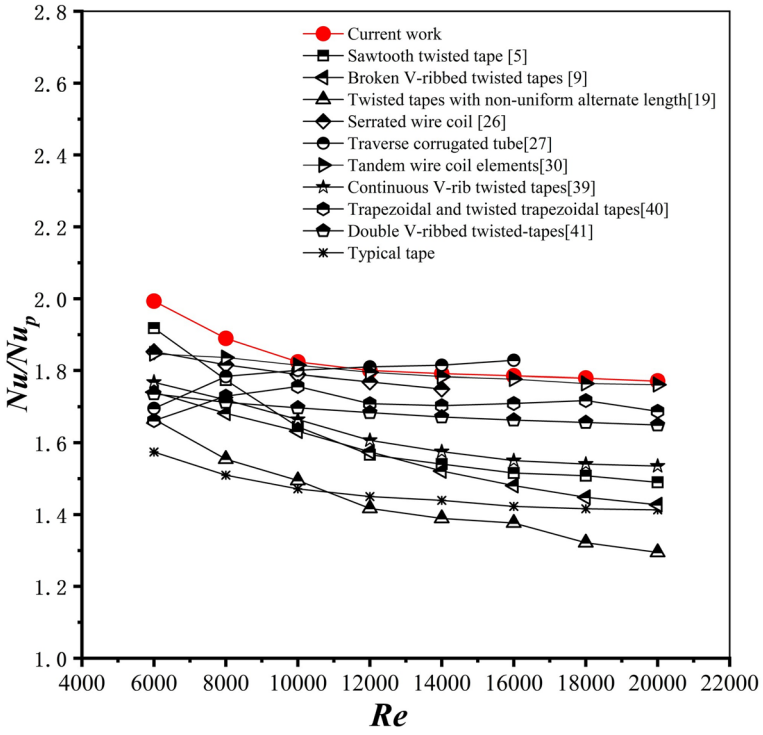

Fig. 17. Comparison of Nu/Nu_p with previous works.

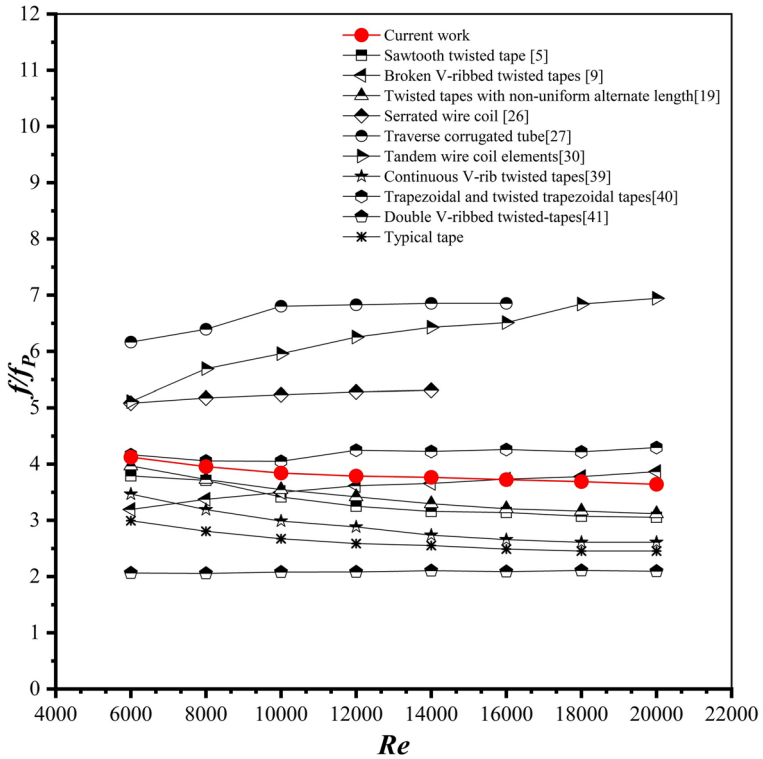

Fig. 18. Comparison of friction factors with previous works.

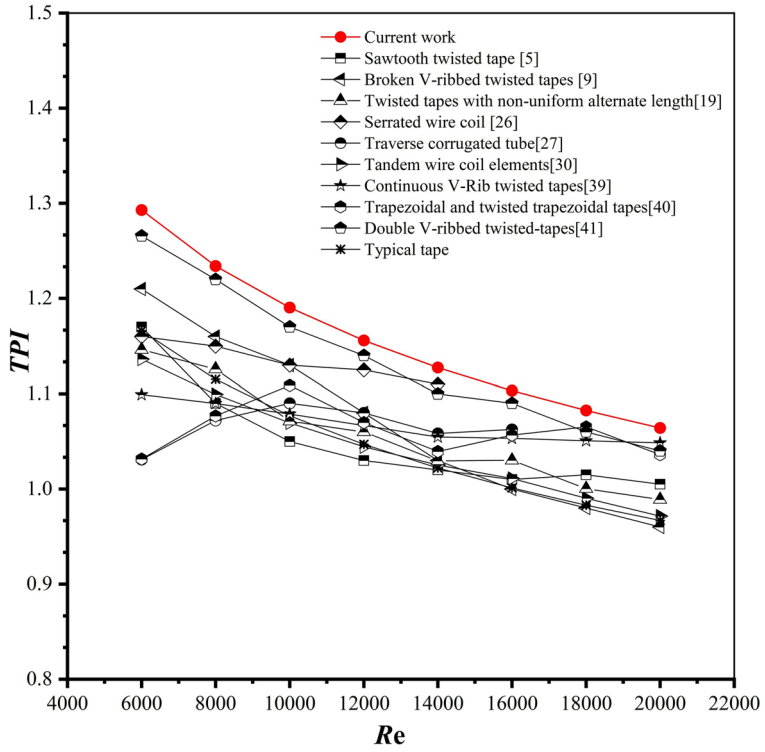

Fig. 19. Comparison of TPI with previous works.

higher than those of the other configurations. These comparisons suggest that the I-rib twisted tape with twisted winglets is the most promising heat transfer enhancement device for energy-efficient applications.

Based on the above research findings, subsequent research will focus on optimization of the I-RTTW geometric structure, aiming to further improve its thermal performance index (TPI) and provide a theoretical basis and technical support for engineering applications of enhanced heat transfer technology.

Conclusions

The flow structure and heat transfer characteristics of heat exchange tubes equipped with I-rib twisted tape and twisted winglets (I-RTTW) were experimentally investigated. The effects of wing depth ratio ($d/W = 0.096$, 0.13, and 0.16) and wing width ratio ($w/W = 0.096$, 0.13, and 0.16) on heat transfer were investigated under turbulent conditions with *Re* values ranging from 6,000 to 20,000. The main research results are as follows:

1. The I-rib twisted tape with twisted winglets (I-RTTW), having a larger wing depth-to-width ratio, generates stronger radial vortices that reduce the thermal boundary layer and radial temperature gradient, thereby significantly enhancing heat transfer efficiency.
2. The I-rib generates longitudinal vortices that enhance boundary layer disruption and fluid mixing, thereby improving thermal performance.
3. At a given Reynolds number, increasing the wing depth and wing width ratios results in enhanced heat transfer and flow resistance. The Nusselt number (*Nu*) increases by a factor of 1.78–1.99 compared to a plain tube, while the friction factor (*f*) rises by 3.76–4.11 times.
4. The TPI reaches a maximum value of 1.29 when both the wing depth ratio (d/W) and wing width ratio (w/W) are 0.16.
5. The deviations the experimental results from the correlation equations for *Nu*, *f*, and TPI and are ± 1.29%, ± 1.55%, and ± 0.17%, respectively, demonstrating the high accuracy of the correlations.
6. This study did not investigate the effects of varying the central I-rib angle or the twist angles of the winglets on heat transfer, friction factor, or thermal performance. Future work will explore these parameters to optimize the balance between heat transfer enhancement and flow resistance, improving TPI and guiding the design of efficient heat exchange equipment.

Data availability

"The datasets generated during the current study are not publicly available due to the deal with National Science, Research and Innovation Fund (NSRF) but are available from the corresponding author on reasonable request."

Received: 28 May 2025; Accepted: 17 September 2025
Published online: 23 October 2025

References

1. Thejaraju, R., Girisha, K. B., Manjunath, S. H. & Dayananda, B. S. Experimental investigation of turbulent flow behavior in an air to air double pipe heat exchanger using novel Para winglet tape. *Case Stud. Therm. Eng.* **22**, 100791 (2020).
2. Altun, A. H., Ors, S. & Dogan, S. Investigation of effects on turbulent heat transfer of twisted wavy tape elements in the tube. *Int. J. Therm. Sci.* **185**, 108068 (2023).
3. International Energy Agency (IEA). *World Energy Outlook 2023* (OECD/IEA, 2023).
4. Rubbi, F., Habib, K., Tusar, M., Das, L. & Rahman, M. T. Numerical study of heat transfer enhancement of turbulent flow using twisted tape insert fitted with hemispherical extruded surface. *Int. J. Heat Technol.* **38**, 314–320 (2020).
5. Samutpraphut, B. et al. Influence of Sawtooth twisted tape on thermal enhancement of heat exchanger tube. *Energy Rep.* **9**, 696–703 (2023).
6. Abdulhamed, A. J., Al-Akam, A., Khudhayer, W. J. & Allw, A. S. Tubular heat enhancement using twisted tape inserts with large holes. *Energy Eng.* **121**, 273–290 (2024).
7. Maradiya, C., Vadher, J. & Agarwal, R. The heat transfer enhancement techniques and their thermal performance factor. *Beni-Suef Univ. J. Basic. Appl. Sci.* **7**, 1–21 (2018).
8. Sedaghat, R., Dalili, K. M. & Hosseinalipour, S. M. A comprehensive analysis of heat transfer in a heat exchanger with simple and perforated twisted tapes based on numerical simulations. *Case Stud. Therm. Eng.* **56**, 104227 (2024).
9. Chuwattanakul, V. et al. Aerothermal performance evaluation of a tube mounted with broken V-ribbed twisted tape: effect of forward/backward arrangement. *Case Stud. Therm. Eng.* **41**, 102642 (2023).
10. Fetuga, I. A. et al. Siqueira, De. O. Thermohydraulic performance of a semi-alternated twisted tape insert and cylindrical baffles in a tube with ternary nanofluid under sinusoidal wall temperature. *Alexandria Eng. J.* **73**, 607–623 (2023).
11. Heeraman, J., Kumar, R., Chaurasiya, P. K., Beloev, H. I. & Iliev, I. K. Experimental evaluation and thermal performance analysis of a twisted tape with dimple configuration in a heat exchanger. *Case Stud. Therm. Eng.* **46**, 103003 (2023).
12. Thapa, S. et al. Analytical investigation of solar parabolic trough receiver with multiple twisted tapes using exergy and energy analysis. *Case Stud. Therm. Eng.* **50**, 103493 (2023).
13. Thote, S. A. & Singh, N. P. Analysis of friction and heat transfer characteristics of tubes with trapezoidal cut twisted tape inserts. *Fluid Dynamics Mater. Process.* **19**, 711–722 (2022).
14. Smaisim, G. F., Gholami, M., Toghraie, D., Hashemian, M. & Abed, A. M. Numerical investigation of the flow and heat transfer of Al_2O_3/water nanofluid in a tube equipped with stationary and self-rotating twisted tapes. *Prog. Nucl. Energy*. **151**, 104335 (2022).
15. Eiamsa-ard, S. et al. Influence of co/counter arrangements of multiple twisted-tape bundles on heat transfer intensification. *Chem. Eng. Process. - Process. Intensif.* **160**, 108304 (2021).
16. Promvonge, P. & Skullong, S. Heat transfer in a tube with combined V-winglet and twin counter-twisted tape. *Case Stud. Therm. Eng.* **26**, 101033 (2021).
17. Luo, C., Song, K. W. & Tagawa, T. Heat transfer enhancement of a double pipe heat exchanger by co-twisting oval pipes with unequal twist pitches. *Case Stud. Therm. Eng.* **28**, 101411 (2021).
18. Eiamsa-ard, S., Nuntadusit, C. & Promvonge, P. Effect of twin delta-winged twisted-tape on thermal performance of heat exchanger tube. *Heat Transfer Eng.* **34**, 1278–1288 (2013).
19. Eiamsa-ard, S., Somkleang, P., Nuntadusit, C. & Thianpong, C. Heat transfer enhancement in tube by inserting uniform/non-uniform twisted-tapes with alternate axes: effect of rotated-axis length. *Appl. Therm. Eng.* **54**, 289–309 (2013).
20. Samruaisin, P., Kunlabud, S., Kunnarak, K., Chuwattanakul, V. & Eiamsa-ard, S. Intensification of convective heat transfer and heat exchanger performance by the combined influence of a twisted tube and twisted tape. *Case Stud. Therm. Eng.* **14**, 100489 (2019).
21. Chang, S. W., Wu, P. S. & Liu, J. H. Aerothermal performance of square duct enhanced by twisted tape with inclined ribs and slots. *Int. J. Heat Mass Transf.* **177**, 121547 (2021).
22. Yu, C. L. et al. Comparative study on turbulent flow characteristics and heat transfer mechanism of a twisted oval tube with different twisted tapes. *Int. J. Therm. Sci.* **174**, 107455 (2022).
23. Abidi, A. et al. Improving the thermal-hydraulic performance of parabolic solar collectors using absorber tubes equipped with perforated twisted tape containing nanofluid. *Sustain. Energy Technol. Assess.* **52**, 102099 (2022).
24. Ghasemian, M., Sheikholeslami, M. & Dehghan, M. Performance improvement of photovoltaic/thermal systems by using twisted tapes in the coolant tubes with different cross-section patterns. *Energy* **279**, 128016 (2013).
25. Chen, P. et al. Analysis of efficiency and performance evaluation criterion of nanofluid flow within a tube enhanced with perforated triple twisted tape: A two-phase analysis. *Case Stud. Therm. Eng.* **48**, 103151 (2013).
26. Chompookham, T., Chingtuaythong, W. & Chokphoemphun, S. Influence of a novel serrated wire coil insert on thermal characteristics and air flow behavior in a tubular heat exchanger. *Int. J. Therm. Sci.* **171**, 107184 (2022).
27. Hong, Y., Du, J., Wang, S., Ye, W. & Huang, S. Turbulent thermal-hydraulic and thermodynamic characteristics in a traverse corrugated tube fitted with twin and triple wire coils. *Int. J. Heat Mass Transf.* **130**, 483–495 (2019).
28. Chithra, V. P. et al. Thermal performance enhancement of laminar flow using compound twisted square duct and variable pitch twisted tape inserts. *Case Stud. Therm. Eng.* **64**, 105462 (2024).
29. Nuntadusit, C., Wae-hayee, M., Bunyajitradulya, A. & Eiamsa-ard, S. Thermal visualization on surface with transverse perforated ribs. *Int. Commun. Heat Mass Transfer*. **39**, 634–639 (2012).
30. Eiamsa-ard, S., Koolnapadol, N. & Promvonge, P. Heat transfer behavior in a square duct with tandem wire coil element insert. *Chin. J. Chem. Eng.* **20**, 863–869 (2012).
31. Pazarlıoğlu, H. K. et al. Numerical simulation of sudden expansion tubes with Ag-MgO nanofluid and innovative fin structure: A thermo-fluidic analysis. *Int. J. Heat Fluid Flow*. **108**, 109448 (2024).
32. Pazarlıoğlu, H. K., Ümit Tepe, A. & ArslanView, K. Thermohydraulic performance assessment of new alternative methods for anti-icing application against current application in an aircraft. *Journal Process. Mech. Engineering* **239**, 3 (2023).
33. Bergles, A. E. & Manglik, R. M. Swirl flow heat transfer and pressure drop with twisted tape inserts, in: J.P. Hartnett, Thomas F Irvine Jr, Young I Cho, George A Greene, Advances in Heat Transfer 36, Academic Press, (2002).
34. Webb, R. L. & Kim, N. H. *Principle of Enhanced Heat Transfer* (Taylor Francis, 1994).
35. Bergman, T. L., Lavine, A. S., Incropera, F. P. & Dewitt, P. D. *Fundamentals of Heat and Mass Transfer* Seventh edn (John Wiley & Sons Inc., 2011).
36. Incropera, F. P., Dewitt, P. D., Bergman, T. L. & Lavine, A. S. *Foundations of Heat Transfer* sixth edn (John Wiley & Sons Inc., 2012).
37. ANSI/ASME. *Measurement Uncertainty: Part 1: Instruments and Apparatus: ANSI/ASME PTC 19.1–1985; American Society of Mechanical Engineers* (New York, NY, USA, 1991).
38. Kline, S. J. & McClintock, F. A. Describing uncertainties in single sample experiments. *Mech. Eng.* **75**, 3–8 (1953).
39. Du, Y. X. et al. Heat transfer intensification in a heat exchanger tube with continuous V-rib twisted tapes installed. *Appl. Sci.* **15**, 10 (2025).
40. Altun, A. H., Nacak, H. & Canli, E. Effect of trapezoidal and twisted trapezoidal tapes on turbulent heat transfer in tubes. *Appl. Therm. Eng.* **211**, 118386 (2022).
41. Tamna, S., Kaewkohkiat, Y., Skullong, S. & Promvonge, P. Heat transfer enhancement in tubular heat exchanger with double V-ribbed twisted-tapes. *Case Stud. Therm. Eng.* **7**, 14–24 (2016).

Author contributions

Wenxuan Qiu; Writing, Draft preparation, Data curation, Validation, Methodology and Formal analysisPrachya Samruaisin, Data curation, Draft preparation, Literature reviewVaresa Chuwattanakul; Writing, Reviewing and EditingNaoki Maruyama; Formal analysisMasafumi Hirota; Formal analysisSmith Eiamsa-ard; Conceptualization, Formal analysisAll authors had approved the final version of the manuscript.

Funding

The Research on "Evaluation of heat transfer performance of a heat exchanger tube mounted with an I-rib twisted tape and twisted winglets" (Grant No. RE-KRIS/FF68/31) by King Mongkut's Institute of Technology, Ladkrabang (KMITL), has received funding support from the NSRF.

Declarations

Competing interests

The authors declare no competing interests.

Additional information

Correspondence and requests for materials should be addressed to V.C.

Reprints and permissions information is available at www.nature.com/reprints.

Publisher's note Springer Nature remains neutral with regard to jurisdictional claims in published maps and institutional affiliations.